DOCUMENTATION OF

CROSS-SHORE NUMERICAL MODEL CSHORE 2009

by

Nobuhisa Kobayashi

RESEARCH REPORT NO. CACR-09-06

NOVEMBER, 2009

CENTER FOR APPLIED COASTAL RESEARCH

Ocean Engineering Laboratory
University of Delaware
Newark, Delaware 19716

ACKNOWLEDGEMENT

TABLE OF CONTENTS

Abstract

ABSTRACT

The majority of the world shoreline is currently suffering from erosion. Beach erosion will become more serious if the mean sea level rise accelerates because of the greenhouse effect. Nourishment and maintenance of wide sand beaches for developed coastal communities will become more expensive unless the present nourishment design method is improved by the development of a reliable morphological model. Concurrently, the recent increase of coastal storm damage demands the development of numerical models for predicting the damage progression and breaching of coastal stone structures and earthen levees during extreme storms. This report summarizes our continuing effort to improve our quantitative understanding of beach morphology and structural damage progression with the goal to develop simple and robust models that are suited for engineering applications. Our effort for the last 10 years has produced the cross-shore numerical model CSHORE which is presently limited to the case of alongshore uniformity. CSHORE consists of the following components: a combined wave and current model based on time-averaged continuity, cross-shore and longshore momentum, wave action, and roller energy equations; a sediment transport model for suspended sand and bedload; a permeable layer model to account for porous flow and energy dissipation; empirical formulas for irregular wave runup; and a probabilistic model for an intermittently wet and dry zone on impermeable and permeable bottoms for the purpose of predicting wave overwash of a dune and armor layer damage progression, respectively. The theories and formulas used in CSHORE are explained in this report in order to facilitate the application of CSHORE to various coastal engineering problems. Finally, the computer program CSHORE is explained so that a user of CSHORE will be able to use it effectively and modify it if necessary. This report of CSHORE2009 updates the earlier report of CSHORE2008 in such a way that a user will not have to read the earlier report.

1. Introduction

A sand beach with a wide berm and a high dune provides storm protection and damage reduction, recreational and economical benefits and biological habitats for plants and animals. Most sandy beaches are eroding partly due to sea level rise. Beach nourishment is widely adopted to maintain a wide beach for a developed coastal community if a suitable beachfill is available in the vicinity of an eroding beach. Empirical methods based on field data have been developed for the design of beach fills (Coastal Engineering Manual 2003). The design of the cross-shore beachfill profile is normally based on the concept of an equilibrium beach profile. The alongshore spreading of the beachfill is generally predicted using a one-line model coupled with the CERC formula or the formula by Kamphuis (1991) for the longshore sediment transport rate. These simple beachfill design methods have been criticized and a number of more process-based models have been proposed. However, the process-based models may not necessarily be more accurate at present.

Sediment transport is caused by the combined action of waves and currents. Our capabilities of predicting wave and current fields have improved steadily for the last 30 years. However, the predictive capability of sediment transport on beaches has not improved much. The major reason for this discrepancy is that no dynamic equation is available to describe the motion of a large number of sediment particles. Consequently, sediment transport models are essentially empirical and dependent on reliable sediment transport data. Unfortunately, sediment dynamics on beaches are highly complex and involve wide ranges of morphological scales in time and space. Correspondingly, available sediment transport models have become more complex and less transparent. We have tried to synthesize available data and formulas in order to develop

simple and transparent formulas for the cross-shore and longshore transport rates of suspended sand and bedload on beaches. The simple formulas need to include basic sediment dynamics sufficiently so that the formulas will be applicable to small-scale and large-scale laboratory beaches as well as natural beaches. Furthermore, the morphological model should be very efficient computationally because the model will need to be calibrated and verified using extensive data sets. The hydrodynamic input required for the morphological model should be limited to the quantities that can be predicted routinely and reliably. These considerations have guided our development of the cross-shore model CSHORE which is presently limited to the conditions of alongshore uniformity and uniform sediment.

Coastal storm damage has been increasing mostly due to the recent growth of coastal population and assets and possibly due to the intensification of hurricanes caused by global warming. Coastal structures including earthen levees (dikes) and rubble mound structures have been designed conventionally for no storm surge overflow and minor wave overtopping during a design storm. Empirical formulas for wave overtopping rates are used for a preliminary design where EurOtop Manual (2007) recommends the latest formulas. Physical model testing is normally conducted in a wave flume or basin for a detailed design. Various numerical models have also been developed to predict detailed hydrodynamics that are difficult to measure even in a laboratory (Kobayashi and Otta 1987; Kobayashi 1999; van Gent 2001). The latest numerical models for hydrodynamics are reviewed by Losada et al. (2008) and Neves et al. (2008). However, our improved predictive capabilities for the hydrodynamics have not really improved our predictive capability for damage progression partly because damage to a coastal structure is cumulative (Melby and Kobayashi 1998). As a result, a performance or risk-based design of a

coastal structure relies on empirical formulas for damage (e.g., Kobayashi et al. 2003). This practical difficulty is similar to that for sediment transport on beaches. Alternatively, the computationally-efficient CSHORE calibrated with extensive data sets has been developed for the design of inclined structures with relatively small wave reflection. Damage progression on the stone armor layer is predicted by modifying the sediment transport model. The eventual goal is to predict the performance of an inclined structure located on a movable bottom.

2. History of CSHORE Development

The history of the cross-shore model CSHORE is summarized to provide an overview of CSHORE and acknowledge a number of graduate students and visiting researchers who contributed to the development of CSHORE. The present version of CSHORE includes the various capabilities added to the initial CSHORE developed in 1998. The different stages of the CSHORE development are summarized in the following where the detail of each stage can be found in the listed publications. The computer program of CSHORE2008 was documented by Kobayashi and Farhadzadeh (2008) and updated in this report for CSHORE2009.

The cross-shore model CSHORE was initially developed to predict the cross-shore transformation of irregular nonlinear waves using the time-averaged continuity, momentum and wave energy equations together with a non-Gaussian probability distribution of the free surface elevation. However, empirical formulas of limited generality were required to parameterize the wave nonlinearity. The present version of CSHORE is based on linear wave theory and the Gaussian probability distribution to reduce the degree of empiricism.

- Kobayashi, N., Herrman, M.N., Johnson, B.D., and Orzech, M.D. (1998). "Probability distribution of surface elevation in surf and swash zones." J. Waterway, Port, Coastal and Ocean Eng., 124(3), 99-107.

- Kobayashi, N., and Johnson, B.D. (1998). "Computer program CSHORE for predicting cross-shore transformation of irregular breaking waves." Res. Rep. No. CACR-98-04, Center for Applied Coastal Research, Univ. of Delaware, Newark, Del.

- Johnson, B.D., and Kobayashi, N. (1998). "Nonlinear time-averaged model in surf and swash zones." Proc. 26th Coastal Eng. Conf., ASCE, 2785-2798.

- Kearney, P.G., and Kobayashi, N. (2000). "Time-averaged probabilistic model for irregular wave runup on coastal structures." Proc. 27th Coastal Eng. Conf., ASCE, 2004-2017.

- Johnson, B.D., and Kobayashi, N. (2000). "Free surface statistics and probabilities in surf zones on beaches." Proc. 27th Coastal Eng. Conf., ASCE, 1022-1035.

The next stage of the CSHORE development was motivated by the need of a computationally-efficient time-averaged model that can be used for the design of porous coastal structures. The linear-wave version of the initial CSHORE was modified to account for the effects of a permeable layer for the case of normally incident waves. The permeable version of CSHORE was called CSHOREP. The impermeable and permeable versions of CSHORE have been merged in the present CSHORE in order to expand the range of practical applications.

- Meigs, L.E., and Kobayashi, N. (2004). "Time-averaged model for irregular breaking waves on porous structures and beaches." Res. Rep. No. CACR-04-02, Center for Applied Coastal Res., Univ. of Delaware, Newark, Del.

- Meigs, L.E., Kobayashi, N., and Melby, J.A. (2004). "Cobble beaches and revetments." Proc. 29th Coastal Eng. Conf., World Scientific, 3865-3877.

- de los Santos, F.J., and Kobayashi, N. (2005). "Irregular wave setup and runup on cobble beaches and revetments." Res. Rep. No. CACR-05-06. Center for Applied Coastal Res., Univ. of Delaware, Newark, Del.

- Ota, T., Kobayashi, N., and Kimura, A. (2006). "Irregular wave transformation over deforming submerged structures." Proc. 30th Coastal Eng. Conf., World Scientific, 4945-4956.

- de los Santos, F.J., Kobayashi, N., and Losada, M. (2006). "Irregular wave runup and overtopping on revetments and cobble beaches." Proc. 30th Coastal Eng. Conf., World Scientific, 4667-4679.

- de los Santos, F.J., and Kobayashi, N. (2006). "Irregular wave seepage and overtopping of cobble beaches and revetments." Res. Rep. No. CACR-06-01, Center for Applied Coastal Res., Univ. of Delaware, Newark, Del.

- Kobayashi, N., Meigs, L.E., Ota, T., and Melby, J.A. (2007). "Irregular breaking wave transmission over submerged porous breakwaters." J. Waterway, Port, Coastal, Ocean Eng., 133(2), 104-116.

- Kobayashi, N., and de los Santos, F.J. (2007). "Irregular wave seepage and overtopping of permeable slopes." J. Waterway, Port, Coastal, Ocean Eng., 133(4), 245-254.

- Ota, T., Matsumi, Y., Kobayashi, N., and Kimura, A. (2007). "Influence of damage progression on performance of rubble mound breakwaters." Proc. Coastal Structures'2007, Venice, Italy, 1806-1817.

- Kobayashi, N., de los Santos, F.J., and Kearney, P.G. (2008). "Time-averaged probabilistic model for irregular wave runup on permeable slopes." J. Waterway, Port, Coastal, Ocean Eng., 134(2), 88-96.

Concurrently, the impermeable version of CSHORE was extended to predict the cross-shore and longshore transport rates of suspended sand and bedload on beaches as a part of the MORPHOS project of the U.S. Army Engineer Research and Development Center. MORPHOS is the world's first attempt at developing an open-source, physics-based computer model of coastal storms and their impact that can be used by the broad coastal community. A series of extensions were made in the following publications to make CSHORE more versatile and better verified.

- Zhao, H., and Kobayashi, N. (2005). "Suspended sand transport in surf zones on equilibrium beaches." Res. Rep. No. CACR-05-01, Center for Applied Coastal Res., Univ. of Delaware, Newark, Del.

- Kobayashi, N., Zhao, H., and Tega, Y. (2005). "Suspended sand transport in surf zone." J. Geophys. Res., 110, C12009, doi:10.1029/2004JC002853.

- Agarwal, A., and Kobayashi, N. (2005). "Time-averaged model for longshore current and sediment transport in surf and swash zones." Res. Rep. No. CACR-05-07, Center for Applied Coastal Res., Univ. of Delaware, Newark, Del.

- Schmied, L., Kobayashi, N., Payo, A., and Puleo, J.A. (2006). "Cross-shore sediment transport and beach profile change." Res. Rep. No. CACR-06-03, Center for Applied Coastal Res., Univ. of Delaware, Newark, Del.

- Schmied, L.D., Kobayashi, N., Puleo, J.A., and Payo, A. (2006). "Cross-shore suspended sand transport on beaches." Proc. 30th Coastal Eng. Conf., World Scientific, 2511-2523.

- Agarwal, A., Kobayashi, N., and Johnson, B.D. (2006). "Longshore suspended sediment transport in surf and swash zones." Proc. 30th Coastal Eng. Conf., World Scientific, 2498-2510.

- Payo, A., Kobayashi, N., and Kim, K.H. (2006). "Beach nourishment strategies." Proc. 30th Coastal Eng. Conf., World Scientific, 4129-4140.

- Kobayashi, N., Agarwal, A., and Johnson, B.D. (2007). "Longshore current and sediment transport on beaches." J. Waterway, Port, Coastal, Ocean Eng., 133(4), 296-304.

- Buck, M., Kobayashi, N., Payo, A., and Johnson, B.D. (2007). "Experiments and numerical model for berm and dune erosion." Res. Rep. No. CACR-07-03, Center for Applied Coastal Res., Univ. of Delaware, Newark, Del.

- Gencarelli, R., Johnson, B.D., Kobayashi, N. and Tomasicchio, G.R. (2007). "Dune erosion and breaching." Proc. Coastal Structures'2007, Venice, Italy, 502-513.

- Kobayashi, N., Payo, A., and Schmied, L. (2008). "Cross-shore suspended sand and bedload transport on beaches." J. Geophys. Res., 113, C07001, doi:10.1029/2007JC004203.

- Kobayashi, N., Buck, M., Payo, A., and Johnson, B.D. (2009). "Berm and dune erosion during a storm." J. Waterway, Port, Coastal, Ocean Eng., 135(1), 1-10.

- Kobayashi, N., Payo, A., and Johnson, B.D. (2009). "Suspended sand and bedload transport on beaches." Handbook of Coastal and Ocean Engineering, World Scientific, Singapore, Chapter 28, 807-823.

- Payo, A., Kobayashi, N., and Yamada, F. (2009). "Suspended sand transport along pier depression." J. Waterway, Port, Coastal, Ocean Eng., 135(5), 245-249.

- Buck, M., Kobayashi, N., Payo, A., and Johnson, B.D. (2008). "Berm and dune erosion." Proc. 31th Coastal Eng. Conf., World Scientific, 1749-1761.

- Gencarelli, R., Tomasicchio, G.R., Kobayashi, N., and Johnson, B.D. (2008). "Beach profile evolution and dune erosion due to the impact of Hurricane Isabel." Proc. 31th Coastal Eng. Conf., World Scientific, 1697-1709.

- Gencarelli, R., Tomasicchio, G.R., Kobayashi, N., and Johnson, B.D. (2008). "Effects of Hurricane Isabel along the North Carolina coastline: Beach profile evolution and dune erosion." Proc. 3rd International Short Conf. on Applied Coastal Res., Lecce, Italy, 200-210.

The following papers summarized the progress of the CSHORE development up to 2008.

- Kobayashi, N. (2006). "Time-averaged wave models for coastal structures and sediments." Proc. 2nd International Short Course and Workshop on Coastal Processes and Port Eng., Cosenza, Italy, 61-75.

- Kobayashi, N., and Farhadzadeh, A. (2008). "Cross-shore numerical model CSHORE for waves, currents, sediment transport and beach profile evolution." Res. Rep. No. CACR-08-01, Center for Applied Coastal Res., Univ. of Delaware, Newark, Del.

- Kobayashi, N. (2009). "Efficient wave and current models for coastal structures and sediments." Nonlinear Wave Dynamics. World Scientific, Singapore, 67-87.

- Kobayashi, N., Figlus, J., and Buck, M. (2009). "Beach nourishment and dune erosion." Proc. 3rd Internal Short Conf. on Applied Coastal Res., Lecce, Italy, 71-98.

The publications above were based on the earlier version of CSHORE limited to the wet zone below the mean water level. In order to extend CSHORE to the zone which is intermittently wet and dry, laboratory experiments were conducted for wave overtopping and overflow on fixed levees. The laboratory data was used for the development of a probabilistic model for the wet

and dry zone on an impermeable bottom. This hydrodynamic model coupled with the sediment transport model in CSHORE has been used to predict wave overwash of dunes. The hydrodynamic model has also been extended to the wet and dry zone on a permeable bottom for the prediction of wave overtopping of rubble mound structures. This model coupled with the CSHORE bedload formula modified for stone has been shown to be capable of predicting the evolution of damaged stone armor layers. The computer program of CSHORE2009 includes these capabilities added in 2009.

- Farhadzadeh, A., Kobayashi, N., Melby, J.A., and Ricottilli, C. (2007). "Experiments and numerical modeling of wave overtopping and overflow on dikes." Res. Rep. No. CACR-07-02, Center for Applied Coastal Res., Univ. of Delaware, Newark, Del.

- Kobayashi, N., Farhadzadeh, A., and Melby, J.A. (2007). "Structures of storm surge disaster prevention." Proc. 4th International Workshop on Coastal Disaster Prevention, Yokohama, Japan, 41-49.

- Farhadzadeh, A., Kobayashi, N., and Melby, J.A. (2008). "Wave overtopping and overflow on inclined structures." Proc. 31st Coastal Eng. Conf., World Scientific, 2996-3008.

- Kobayashi, N., Farhadzadeh, A., Melby, J.A., Johnson, B., and Gravens, M. (2010). "Wave overtopping of levees and overwash of dunes." J. Coastal Research (in press).

- Kobayashi, N., and Farhadzadeh, A. (2009). "Dune erosion and overwash." Proc. Coastal Dynamics 2009, Tokyo, Japan, Paper No. 81.

- Johnson, B., Gravens, M., Wamsley, T., and Kobayashi, N. (2009). "A predictive model for beach profile evolution." Proc. Coastal Dynamics 2009, Tokyo, Japan, Paper No. 64.

- Johnson, B., Seymour, R., and Kobayashi, N. (2009). "A profile evolution model including erosion and accretion." 2009 National Conf., American Shore and Beach Preservation Association, St. Pete Beach, Florida.

- Figlus, J., Kobayashi, N., Gralher, C., and Iranzo, V. (2009). "Experimental and numerical study on transition from minor to major wave overwash of dunes." Res. Rep. No. CACR-09-04, Center for Applied Coastal Res., Univ. of Delaware, Newark, Del.

- Figlus, J., Kobayashi, N., Gralher, C., and Iranzo, V. (2009). "Wave-induced overwash and destruction of sand dunes." 32nd Coastal Eng. Conf., World Scientific, (submitted).

- Figlus, J., Kobayashi, N., Gralher, C., and Iranzo, V. (2009). "Wave overtopping and overwash of dunes." J. Waterway, Port, Coastal, Ocean Eng., (submitted).

- Farhadzadeh, A., Kobayashi, N., and Melby, J.A. (2009). "Wave overtopping and damage progression on rubble mound structures." Res. Rep. No. CACR-09-05, Center for Applied Coastal Res., Univ. of Delaware, Newark, Del.

- Farhadzadeh, A., Kobayashi, N., and Melby, J.A. (2009). "Evolution of damaged armor layer profile." 32nd Coastal Eng. Conf., World Scientific, (submitted).

- Hicks, B., Kobayashi, N., Puleo, J., and Farhadzadeh, A. (2009). "Cross-shore gravel transport on beaches." 32nd Coastal Eng. Conf., World Scientific, (submitted).

- Kobayashi, N., Farhadzadeh, A., and Melby, J.A. (2009). "Wave action and damage on stone structures." J. Waterway, Port, Coastal, Ocean Eng., (submitted).

In addition, CSHORE will be extended to predict the long-term (seasonal and yearly) cross-shore and longshore sediment transport rates on natural and nourished beaches. The field data required

for the calibration and verification for the long-term morphological model CSHORE has been obtained and analyzed in the following publications:

- Figlus, J., and Kobayashi, N. (2007). "Seasonal and yearly profile changes of Delaware beaches." Res. Rep. No. CACR-07-01, Center for Applied Coastal Res., Univ. of Delaware, Newark, Del.

- Figlus, J., and Kobayashi, N. (2008). "Inverse estimation of sand transport rates on nourished Delaware beaches." J. Waterway, Port, Coastal, Ocean Eng., 134(4), 218-225.

- Figlus, J., and Kobayashi, N. (2008). "Two-line model for inverse estimation of cross-shore and longshore transport rates on nourished beaches." 31st Coastal Eng. Conf., World Scientific, 2545-2556.

3. Wave and Current Models

Cross-shore sediment transport on beaches has been investigated extensively (e.g., Kriebel and Dean 1985; van Rijn et al. 2003) but we still cannot predict beach profile evolution accurately. In order to improve our predictive capabilities, sediment transport models have become more sophisticated but less transparent. For example, Thornton et al. (1996) and Gallagher et al. (1998) used the energetics-based total load model of Bailard (1981) to explain the offshore movement of a bar at Duck, North Carolina during storms. The onshore bar migration on the same beach was predicted by both Hoefel and Elgar (2003), using the skewed acceleration effect on bedload, and Henderson et al. (2004), using a suspended sediment model. The roles of bedload and suspended load are not clear at present. Kobayashi et al. (2008a) made an attempt to synthesize and simplify existing cross-shore sediment transport models with the aim of developing a simple and robust model that is suited for engineering applications including the

berm and dune erosion. This model has been extended to predict the cross-shore and longshore transport rates of bedload and suspended load under the combined wave and current action (Kobayashi et al. 2007a; 2009b).

Sediment transport on beaches is caused by the combined action of waves and currents. The hydrodynamic input required for a sediment transport model depends on whether the sediment transport model is time-dependent (phase-resolving) or time-averaged over a number of waves. A time-dependent sediment transport model such as that by Kobayashi and Johnson (2001) is physically appealing because it predicts intense but intermittent sand suspension under irregular breaking waves (Kobayashi and Tega 2002). However, the time-dependent model requires considerable computation time and is not necessarily more accurate in predicting slow morphological changes than the corresponding time-averaged model presented in the following. Horizontally two-dimensional wave and current models are presented first before the cross-shore model CSHORE based on the assumption of alongshore uniformity.

Fig. 1 shows obliquely incident irregular waves on an essentially straight shoreline where the cross-shore coordinate x is positive onshore and the longshore coordinate y is positive in the downwave direction. The beach is assumed to be impermeable. The depth-averaged cross-shore and longshore velocities are denoted by U and V, respectively. Incident waves are assumed to be unidirectional with θ = incident angle relative to the shore normal. The height and period of the irregular waves are represented by the root-mean-square wave height H_{rms} and the representative wave period, which is taken as the spectral peak period T_p, specified at the seaward boundary located at $x = 0$. The location of the seaward boundary is normally taken to be outside the surf

zone so that wave set-down or setup is very small at $x=0$. The incident wave angle θ at $x=0$ is assumed to be in the range of $|\theta| < 80°$ to ensure that the incident waves propagate landward. The wind speed and direction at the elevation of 10 m above the sea surface are denoted by W_{10} and θ_w, respectively.
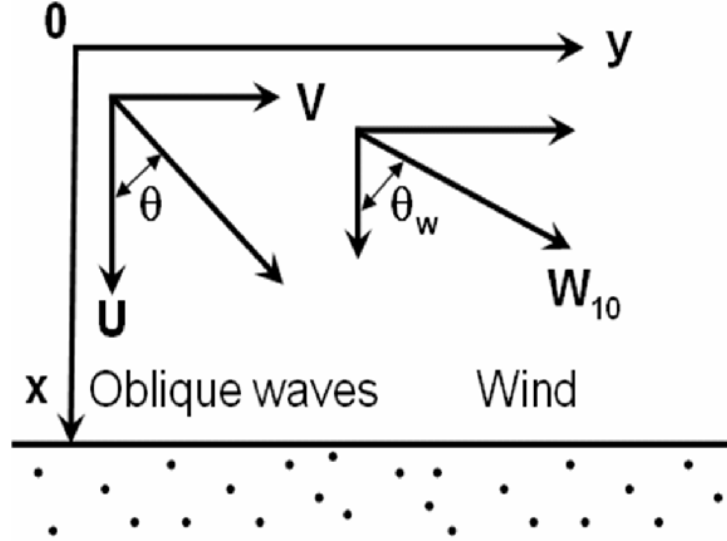
Fig. 1. Definition sketch for incident irregular waves and wind on beach.

The mean water depth $\bar{h}$ is given by

$$\bar{h} = \left(\bar{\eta} + S - z_b \right) \tag{1}$$

where $\bar{\eta}$ = wave setup above the still water level (SWL); and S = storm tide above the datum $z = 0$ which is assumed to be uniform in the computation domain and is specified as input at $x=0$. Linear wave and current theory for wave refraction (e.g., Phillips 1977; Mei 1989; Dalrymple 1988) is used to predict the spatial variations of H_{rms} and θ. The dispersion relation for linear waves is expressed as

16

$$\omega^2 = kg\tanh\left(k\overline{h}\right) \quad ; \quad \omega_p = \omega + k\left(Q_x\cos\theta + Q_y\sin\theta\right)/\overline{h} \qquad (2)$$

where ω = intrinsic angular frequency; k = wave number; g = gravitational acceleration; $\overline{h}$ = mean water depth with the overbar indicating time-averaging; ω_p = absolute angular frequency given by $\omega_p = 2\pi/T_p$; Q_x and Q_y = time-averaged volume flux per unit width in the x and y directions, respectively, and θ = incident wave angle. Eq. (2) can be solved iteratively to obtain k and ω for known $\omega_p, \overline{h}, \theta, Q_x$ and Q_y. The phase velocity C and the group velocity C_g are given by

$$C = \omega/k \quad ; \quad C_g = nC \quad ; \quad n = \frac{1}{2}\left[1 + \frac{2k\overline{h}}{\sinh\left(2k\overline{h}\right)}\right] \qquad (3)$$

The wave angle θ is computed using the irrotationality of the wave number

$$\frac{\partial}{\partial x}(k\sin\theta) - \frac{\partial}{\partial y}(k\sin\theta) = 0 \qquad (4)$$

The root-mean-square wave height H_{rms} defined as $H_{rms} = \sqrt{8}\,\sigma_\eta$ with σ_η = standard deviation of the free surface elevation η which is computed using the wave action equation

$$\frac{\partial}{\partial x}\left[\frac{E}{\omega}\left(C_g\cos\theta + \frac{Q_x}{\overline{h}}\right)\right] + \frac{\partial}{\partial y}\left[\frac{E}{\omega}\left(C_g\sin\theta + \frac{Q_y}{\overline{h}}\right)\right] = -\frac{D_B + D_f}{\omega} \qquad (5)$$

with

$$E = \rho g\sigma_\eta^2 = \frac{1}{8}\rho g H_{rms}^2 \qquad (6)$$

where E = specific wave energy; ρ = fluid density; and D_B and D_f = wave energy dissipation rate per unit horizontal area due to wave breaking and bottom friction, respectively. The formulas for D_B and D_f are presented later in relation to the cross-shore model CSHORE.

The time-averaged volume fluxes Q_x and Q_y in Eq. (2) are expressed as

$$Q_x = \overline{h}\,\overline{U} + Q_{wx} \quad ; \quad Q_y = \overline{h}\,\overline{V} + Q_{wy} \tag{7}$$

with

$$Q_{wx} = \frac{g\sigma_\eta^2 \cos\theta}{C} + q_r \cos\theta \quad ; \quad Q_{wy} = \frac{g\sigma_\eta^2 \sin\theta}{C} + q_r \sin\theta \tag{8}$$

where $\overline{U}$ and $\overline{V}$ = time-averaged, depth-averaged velocities in the x and y directions; Q_{wx} and Q_{wy} = wave-induced volume fluxes in the x and y directions; $\left(g\sigma_\eta^2/C\right)$ = volume flux due to linear waves propagating in the direction of θ; and q_r = volume flux of a roller on the front of a breaking wave. The roller volume flux q_r is estimated using the roller energy equation as explained by Kobayashi et al. (2005,2007a)

$$\frac{\partial}{\partial x}\left(\rho C^2 q_r \cos\theta\right) + \frac{\partial}{\partial y}\left(\rho C^2 q_r \sin\theta\right) = D_B - D_r \tag{9}$$

with

$$D_r = \rho g \beta_r q_r \quad ; \quad \beta_r = \left(0.1 + S_b\right) \geq 0.1 \tag{10}$$

$$S_b = \frac{\partial z_b}{\partial x}\cos\theta + \frac{\partial z_b}{\partial y}\sin\theta \tag{11}$$

where D_r = roller dissipation rate; β_r = wave-front slope; S_b = bottom slope in the direction of wave propagation; and z_b = bottom elevation relative to the datum $z = 0$ with z = vertical coordinate taken to be positive upward. The wave front slope β_r is assumed to be 0.1 unless it is increased by the positive bottom slope S_b.

18

The mean water depth $\bar{h}$ and the current velocities $\bar{U}$ and $\bar{V}$ are computed using the time-averaged continuity and momentum equations (Phillips 1977; Svendsen et al. 2002).

$$\frac{\partial}{\partial x}(Q_x) + \frac{\partial}{\partial y}(Q_y) = 0 \tag{12}$$

$$\frac{\partial}{\partial x}\left(\frac{Q_x^2}{\bar{h}}\right) + \frac{\partial}{\partial y}\left(\frac{Q_x Q_y}{\bar{h}}\right) + g\bar{h}\frac{\partial\bar{\eta}}{\partial x} + \frac{\tau_{bx}}{\rho} = \tau_{wx} + \frac{\tau_{sx}}{\rho} \tag{13}$$

$$\frac{\partial}{\partial x}\left(\frac{Q_x Q_y}{\bar{h}}\right) + \frac{\partial}{\partial y}\left(\frac{Q_y^2}{\bar{h}}\right) + g\bar{h}\frac{\partial\bar{\eta}}{\partial y} + \frac{\tau_{by}}{\rho} = \tau_{wy} + \frac{\tau_{sy}}{\rho} \tag{14}$$

with

$$\tau_{wx} = -\frac{\partial}{\partial x}\left(\frac{S_{xx}}{\rho} - \frac{Q_{wx}^2}{\bar{h}}\right) - \frac{\partial}{\partial y}\left(\frac{S_{xy}}{\rho} - \frac{Q_{wx}Q_{wy}}{\bar{h}}\right) \tag{15}$$

$$\tau_{wy} = -\frac{\partial}{\partial x}\left(\frac{S_{xy}}{\rho} - \frac{Q_{wx}Q_{wy}}{\bar{h}}\right) - \frac{\partial}{\partial y}\left(\frac{S_{yy}}{\rho} - \frac{Q_{wy}^2}{\bar{h}}\right) \tag{16}$$

$$S_{xx} = (nE + M_r)\cos^2\theta + E\left(n - \frac{1}{2}\right) \quad ; \quad M_r = \rho C q_r \tag{17}$$

$$S_{xy} = (nE + M_r)\cos\theta\sin\theta \quad ; \quad S_{yy} = (nE + M_r)\sin^2\theta + E\left(n - \frac{1}{2}\right) \tag{18}$$

where τ_{bx} and τ_{by} = bottom shear stresses in the x and y directions; τ_{sx} and τ_{sy} = wind stresses on the sea surface in the x and y directions; and S_{xx}, S_{xy} and S_{yy} = radiation stresses including the momentum flux M_r of a roller propagating with the phase speed C. It is noted that the terms

19

$Q_{wx}^2, Q_{wx}Q_{wy}$ and Q_{wy}^2 in Eqs. (15) and (16) included by Phillips (1977) are of 4-th order in terms of the wave height and normally neglected. The present circulation model based on Eqs. (12) – (18) is a simplified version of SHORECIRC (Svendsen et al. 2002) for irregular waves where SHORECIRC assumes monochromatic waves. The formulas for τ_{bx}, τ_{by}, τ_{sx} and τ_{sy} are presented later in relation to the cross-shore model CSHORE.

A horizontally two-dimensional model C2SHORE has been developed in the MORPHOS project (Shi et al. 2008). The directional spectral wave model STWAVE (Smith et al. 2001) is used to predict the wave transformation. The wave-induced fluxes Q_{wx} and Q_{wy} and the radiation stresses S_{xx}, S_{xy} and S_{yy} are computed from the predicted directional wave spectra. The roller effects included in Eqs. (8), (17) and (18) are neglected. The circulation model is based on Eqs. (12)– (16) with the formulas for τ_{bx}, τ_{by}, τ_{sx} and τ_{sy} used in CSHORE. The wave and circulation models are coupled and run iteratively for several times. The wave field is computed to estimate τ_{wx} and τ_{wy} given by Eqs. (15) and (16) for the circulation model which computes the wave setup and wave-induced currents. An efficient finite difference method is used to solve Eqs. (12) – (14) and reduce the computation time considerably (Shi et al. 2007). The iteration between the wave and circulation models is necessary in the region near and landward of the still water shoreline where wave setup determines the mean water depth $\bar{h}$ for the wave model. The wave and current models in Section 3 are limited to the wet zone below the mean water level. Shi et al. (2008) compared C2SHORE with the morphological change data at the U.S. Army Corps of Engineers Field Research Facility (FRF) during Hurricane Isabel and found the need to include the effects of the FRF piling.

4. Combined Wave and Current Model CSHORE in Wet Zone

The cross-shore model CSHORE assumes alongshore uniformity but computes the wave and current fields simultaneously. The depth-integrated continuity equation of water given by Eq. (12) requires that the cross-shore volume flux Q_x is constant and equal to the wave overtopping rate q_o at the landward end of the computation domain. Eqs. (7) and (8) yield

$$Q_x = \overline{h}\,\overline{U} + \frac{g\sigma_\eta^2}{C}\cos\theta + q_r\cos\theta = q_o \tag{19}$$

$$Q_y = \overline{h}\,\overline{V} + \frac{g\sigma_\eta^2}{C}\sin\theta + q_r\sin\theta \tag{20}$$

where $\overline{h}$ = mean water depth; $\overline{U}$ = mean cross-shore velocity; which is negative and offshore because $\cos\theta > 0$ if $q_o = 0$ (no wave overtopping); g = gravitational acceleration; σ_η = standard deviation of the free surface elevation η; C = linear wave phase velocity in the mean water depth $\overline{h}$ corresponding to the spectral peak period T_p; and q_r = volume flux of a roller on the front of a breaking wave. If the incident wave angle θ is small, Eq. (20) can be approximated by $Q_y \simeq \overline{h}\,\overline{V}$ for most applications.

For the case of alongshore uniformity, Eq. (4) reduces to Snell's law which is used to obtain the wave direction θ

$$k\sin\theta = \text{constant} \tag{21}$$

The constant value is obtained from the values of θ, $\overline{h}$ and T_p specified at the seaward boundary $x = 0$ located outside the surf zone where ω can be approximated by ω_p in Eq. (2). Reflected waves are neglected in this model.

The cross-shore and longshore momentum equations (13) and (14) are simplified as

$$\frac{d}{dx}\left(S_{xx} + \rho\frac{Q_x^2}{\bar{h}}\right) = -\rho g\bar{h}\frac{d\bar{\eta}}{dx} - \tau_{bx} + \tau_{sx} \tag{22}$$

$$\frac{d}{dx}\left(S_{xy} + \rho\frac{Q_x Q_y}{\bar{h}}\right) = -\tau_{by} + \tau_{sy} \tag{23}$$

where S_{xx} = cross-shore radiation stress; ρ = water density; τ_{bx} = cross-shore bottom stress; τ_{sx} = cross-shore wind stress on the sea surface; S_{xy} = shear component of the radiation stress; τ_{by} = longshore bottom stress; and τ_{sy} = longshore wind stress on the sea surface. The wind shear stresses may not be negligible especially outside surf zones on natural beaches (Lentz et al. 1999). Linear wave theory for progressive waves is used to estimate S_{xx} and S_{xy} as in Eqs. (17) and (18)

$$S_{xx} = (nE + M_r)\cos^2\theta + E\left(n - \frac{1}{2}\right) \;;\; S_{xy} = (nE + M_r)\cos\theta\sin\theta \tag{24}$$

with

$$n = C_g / C \;;\quad E = \rho g\sigma_\eta^2 \;;\quad M_r = \rho C q_r \tag{25}$$

where C_g = linear wave group velocity; E = specific wave energy with the root-mean-square wave height defined as $H_{rms} = \sqrt{8}\,\sigma_\eta$; and M_r = momentum flux of a roller propagating with the phase velocity C. It is noted that the equations used in CSHORE are presented again for clarity.

The time-averaged bottom shear stresses in Eqs. (22) and (23) are written as

$$\tau_{bx} = \frac{1}{2}\rho f_b \overline{UU_a} \quad ; \quad \tau_{by} = \frac{1}{2}\rho f_b \overline{VU_a} \quad ; \quad U_a = \left(U^2 + V^2\right)^{0.5} \tag{26}$$

where U = depth-averaged cross-shore velocity; V = depth-averaged longshore velocity; f_b = bottom friction factor; and the overbar indicates time averaging. The bottom friction factor f_b is of the order of 0.01 on sand beaches but should be calibrated using longshore current data because of the sensitivity of longshore currents to f_b. The equivalency of the time and probabilistic averaging is assumed to express τ_{bx} and τ_{by} in terms of the mean and standard deviation of the depth-averaged velocities U and V expressed as

$$U = \sigma_T F_U \quad ; \quad V = \sigma_T F_V \quad ; \quad U_a = \sigma_T F_a \quad ; \quad F_a = \left(F_U^2 + F_V^2\right)^{0.5} \tag{27}$$

with

$$F_U = U_* + r\cos\theta \quad ; \quad F_V = V_* + r\sin\theta \quad ; \quad U_* = \frac{\overline{U}}{\sigma_T} \quad ; \quad V_* = \frac{\overline{V}}{\sigma_T} \tag{28}$$

where $\overline{U}$ and $\overline{V}$ = depth-averaged cross-shore and longshore currents; σ_T = standard deviation of the oscillatory (assumed Gaussian) depth-averaged velocity U_T with zero mean; and r = Gaussian variable defined as $r = U_T/\sigma_T$ whose probability density function is given by

$$f(r) = \frac{1}{\sqrt{2\pi}} \exp\left(-\frac{r^2}{2}\right) \tag{29}$$

Linear progressive wave theory is used locally to express U_T in terms of the oscillatory free surface elevation $\left(\eta - \overline{\eta}\right)$

$$U_T = \frac{C}{\overline{h}}\left(\eta - \overline{\eta}\right) \tag{30}$$

which yields the standard deviation σ_T of the oscillatory velocity U_T

23

$$\sigma_T = C\sigma_* \quad ; \quad \sigma_* = \sigma_\eta / \bar{h} \tag{31}$$

It is noted that that $U_* = \bar{U}/\sigma_T$ and $V_* = \bar{V}/\sigma_T$ are of the order of unity or less. The standard deviations of U and V are given by

$$\sigma_U = \sigma_T \cos\theta \quad ; \quad \sigma_V = \sigma_T |\sin\theta| \tag{32}$$

where $\cos\theta > 0$ but $\sin\theta$ can be negative. Substitution of Eq. (27) into Eq. (26) yields

$$\tau_{bx} = \frac{1}{2}\rho f_b \sigma_T^2 G_{bx} \quad ; \quad \tau_{by} = \frac{1}{2}\rho f_b \sigma_T^2 G_{by} \tag{33}$$

with

$$G_{bx} = \int_{-\infty}^{\infty} F_U F_a f(r)dr \quad ; \quad G_{by} = \int_{-\infty}^{\infty} F_V F_a f(r)dr \tag{34}$$

which must be integrated numerically.

The wind shear stress in Eqs. (22) and (23) are expressed as

$$\tau_{sx} = \rho_a C_D W_{10}^2 \cos\theta_w \quad ; \quad \tau_{sy} = \rho_a C_D W_{10}^2 \sin\theta_w \tag{35}$$

where ρ_a = air density ($\rho_a \simeq 1.225$ kg/m^3); C_D = drag coefficient, W_{10} = 10-m wind speed; and θ_w = wind direction defined in Fig. 1. The formula by Large and Pond (1981) is used to estimate C_D where $C_D = 0.0012$ for $W_{10} < 11$ m/s and $C_D = (0.00049 + 0.000065\,W_{10})$ for $W_{10} \geq 11$ m/s. It is noted that the measured values of C_D during tropical cyclones by Powell et al. (2003) indicated no increase of C_D with the increase of W_{10} much above 25 m/s. In short, available data is insufficient to estimate C_D for extreme wind conditions.

24

The wave action equation (5) for the case of alongshore uniformity becomes

$$\frac{d}{dx}\left[\frac{E}{\omega}\left(C_g\cos\theta+\frac{Q_x}{\overline{h}}\right)\right]=-\frac{D_B+D_f}{\omega} \tag{36}$$

which reduces to the wave energy equation if ω is constant and $Q_x=0$.

$$\frac{dF_x}{dx}=-D_B-D_f \quad ; \quad F_x=EC_g\cos\theta \tag{37}$$

where F_x = cross-shore energy flux based on linear progressive wave theory; and D_B and D_f = energy dissipation rates due to wave breaking and bottom friction, respectively.

The energy dissipation rate D_B due to wave breaking in Eq. (36) is estimated using the formula by Battjes and Stive (1985), which was modified by Kobayashi et al. (2005) to account for the local bottom slope and to extend the computation to the lower swash zone. The modified formula is expressed as

$$D_B=\frac{\rho g a_s Q H_B^2}{4T} \quad ; \quad \frac{Q-1}{\ell n Q}=\left(\frac{H_{rms}}{H_m}\right)^2 \quad ;$$

$$H_m=\frac{0.88}{k}\tanh\left(\frac{\gamma k\overline{h}}{0.88}\right) \quad ; \quad a_s=\frac{2\pi S_b}{3k\overline{h}}\geq1 \tag{38}$$

where a_s = slope effect parameter; Q = fraction of breaking waves; H_B = breaker height used to estimate D_B; T = intrinsic wave period given by $T=2\pi/\omega$ with ω obtained using Eq. (2); $H_{rms}=\sqrt{8}\sigma_\eta$ = local root-mean-square wave height; H_m = local depth-limited wave height; k = wave number; $\overline{h}$ = mean water depth including wave setup; γ = empirical breaker ratio

parameter; and S_b = local bottom slope given by Eq. (11). The parameter a_s is the ratio between the wave length $(2\pi/k)$ and the horizontal length $(3\bar{h}/S_b)$ imposed by the small depth and relatively steep slope where the lower limit of $a_s = 1$ corresponds to the formula by Battjes and Stive (1985) who also assumed $H_B = H_m$. The fraction Q is zero for no wave breaking and unity when all waves break. The requirement of $0 \le Q \le 1$ implies $H_{rms} \le H_m$ but H_{rms} can become larger than H_m in very shallow water. When $H_{rms} > H_m$, use is made of $Q = 1$ and $H_B = H_{rms}$. In addition, the upper limit of $\sigma_* = \sigma_\eta/\bar{h}$ is imposed as $\sigma_* \le 1$ in very shallow water (Kobayashi et al. 1998). The breaker ratio parameter γ in Eq. (38) is typically in the range of $\gamma = 0.5 - 1.0$ (Kobayashi et al. 2007a) but should be calibrated to obtain a good agreement with the measured cross-shore variation of σ_η if such data is available. An option is provided in CSHORE2009 to estimate γ using the empirical formula developed by Apotsos et al. (2008) using field data.

On the other hand, the energy dissipation rate D_f due to bottom friction in Eq. (36) is expressed as

$$D_f = \frac{1}{2}\rho f_b \overline{U_a^3} \tag{39}$$

Substitution of U_a given in Eq. (27) into Eq. (39) yields

$$D_f = \frac{1}{2}\rho f_b \sigma_T^3 G_f \quad ; \quad G_f = \int_{-\infty}^{\infty} F_a^3 f(r)dr \tag{40}$$

where $f(r)$ is given by Eq. (29).

The energy equation for the roller given by Eq. (9) reduces to that used by Ruessink et al. (2001) for the case of alongshore uniformity

$$\frac{d}{dx}\left(\rho C^2 q_r \cos\theta\right) = D_B - D_r \quad ; \quad D_r = \rho g \beta_r q_r \tag{41}$$

where the roller dissipation rate D_r is assumed to equal the rate of work to maintain the roller on the wave-front slope β_r of the order of 0.1. Use is made of the empirical formula given by Eq. (10) proposed by Kobayashi et al. (2005) who included the local bottom slope effect. If the roller is neglected, $q_r = 0$ and Eq. (41) yields $D_r = D_B$. The roller effect improves the agreement for the longshore current (Kobayashi et al. 2007a).

Eqs. (19) – (41) are the same as those used by Kobayashi et al. (2007a) who assumed $Q_x = q_o = 0$ in Eq. (19) and neglected the wind shear stresses in Eqs. (22) and (23), and used linear shallow-water wave theory with $C = (g\bar{h})^{0.5}$ in Eq. (30). Substitution of Eqs. (31) and (32) into Eq. (19) yields the following equation of the mean cross-shore current:

$$\overline{U} = -\frac{g\bar{h}}{C^2}\sigma_U \sigma_* \left(1 + \frac{Cq_r}{g\sigma_\eta^2}\right) + \frac{Q_x}{\bar{h}} \tag{42}$$

The landward-marching computation starting from $x = 0$ outside the surf zone is the same as that of Kobayashi et al. (2007a).

Approximate analytical equations of G_{bx}, G_{by} and G_f given by Eqs. (34) and (40) are obtained by Kobayashi (2009a) to reduce the computation time and improve the numerical stability. The function F_a given in Eq. (27) with Eq. (28) is rewritten as

$$F_a = \left[\left(r - r_m\right)^2 + F_m^2\right]^{0.5} \tag{43}$$

with

$$r_m = -(U_* \cos\theta + V_* \sin\theta) \quad ; \quad F_m = V_* \cos\theta - U_* \sin\theta \tag{44}$$

Eq. (43) is approximated as

$$F_a = (r - r_m) + |F_m| \quad \text{for} \quad r \ge 0$$

$$F_a = -(r - r_m) + |F_m| \quad \text{for} \quad r < 0 \tag{45}$$

Substituting Eq. (45) into Eqs. (34) and (40) and integrating the resulting equations analytically, we obtain approximate expressions for G_{bx}, G_{by} and G_f

$$G_{bx} = \sqrt{\frac{2}{\pi}}\left(U_* - r_m \cos\theta\right) + U_* |F_m| \tag{46}$$

$$G_{by} = \sqrt{\frac{2}{\pi}}\left(V_* - r_m \sin\theta\right) + V_* |F_m| \tag{47}$$

$$G_f = 2\sqrt{\frac{2}{\pi}} + \left(1 + U_*^2 + V_*^2\right)|F_m| + \sqrt{\frac{2}{\pi}}\left(U_*^2 + V_*^2 + 2r_m^2\right) \tag{48}$$

which depends on $\sin\theta$ ($\cos\theta > 0$ assumed), r_m and F_m where Eq. (44) yields $U_* = -(r_m \cos\theta + F_m \sin\theta)$ and $V_* = (F_m \cos\theta - r_m \sin\theta)$.

For the case of normally incident waves with no wind, $\sin\theta = 0$ and $V_* = 0$. Eqs. (46) – (48) yield $G_{bx} = 1.6\ U_*$, $G_{by} = 0$, and $G_f = (1.6 + 2.4\ U_*^2)$. For this case, Eq. (23) requires $\tau_{by} = 0$ for $Q_x = 0$ (no wave overtopping) and Eq. (33) yields $G_{by} = 0$. As a result, Eq. (47) is exact. For $\sin\theta = 0$ and $V_* = 0$, G_{bx} and G_f given by Eqs. (34) and (40) can be integrated analytically as presented by Kobayashi et al. (2007b) who approximated the analytical expressions of G_{bx} and G_f as $G_{bx} = 1.64\ U_*$ and $G_f = (1.6 + 2.6\ U_*^2)$. These approximate equations are very similar to the above equations obtained from Eqs. (46) and (48). For the case of $|\sin\theta| \ll 1$ and $|U_*| \ll |V_*|$,

28

Eq. (47) can be approximated as $G_{by} = V_* (0.8 + |V_*|)$. Using field data and probabilistic analyses, Feddersen et al. (2000) obtained $G_{by} = V_* (1.16^2 + V_*^2)^{0.5}$. The difference between these two approximate equations for G_{by} is less than 20% for $|V_*| < 1.4$, which is typically satisfied.

Kobayashi et al. (2009a) compared the approximate values of G_{bx}, G_{by} and G_f given by Eqs. (46) – (48) with the exact values of G_{bx}, G_{by} and G_f obtained by the numerical integration of Eqs. (34) and (40). The percentage error was typically about 10% and always less than 35% for the ranges of $|\sin \theta| < 1$, $|r_m| < 1$ and $|F_m| < 1$. This error is probably less than the uncertainty of the bottom friction factor f_b.

5. Sediment Transport Model in Wet Zone

The combined wave and current model CSHORE predicts the spatial variations of the hydrodynamic variables used in the following sediment transport model for given beach profile, water level and seaward wave conditions at $x = 0$. The bottom sediment is assumed to be uniform and characterized by d_{50} = median diameter; w_f = sediment fall velocity; and s = sediment specific gravity. The sediment transport model developed for CSHORE is modified slightly in the following for the horizontally two-dimensional model C2SHORE.

First, the spatial variation of the degree of sediment movement is estimated using the critical Shields parameter ψ_c (Madsen and Grant 1976) which is taken as $\psi_c = 0.05$. The instantaneous bottom shear stress τ'_b is assumed to be given by $\tau'_b = 0.5 \rho f_b U_a^2$ with U_a given in Eq. (26). The sediment movement is assumed to occur when τ'_b exceeds the critical shear stress, $\rho g(s-1)d_{50} \psi_c$.

29

The probability P_b of sediment movement can be shown to be the same as the probability of

$(r - r_m)^2 > F_b^2 = (R_b^2 - F_m^2)$ where $R_b = [2 \ g \ (s-1) \ d_{50} \ \psi_c \ f_b^{-1}]^{0.5}/\sigma_T$ and r_m and F_m are defined in

Eq. (44). For the Gaussian variable r given by Eq. (29), P_b is given by

$$P_b = \frac{1}{2} erfc\left(\frac{F_b - r_m}{\sqrt{2}}\right) + \frac{1}{2} erfc\left(\frac{F_b + r_m}{\sqrt{2}}\right) \quad \text{for} \quad F_b^2 > 0 \qquad (49)$$

and $P_b = 1$ for $F_b^2 \leq 0$ where erfc is the complementary error function. The value of P_b

computed from $x = 0$ located outside the surf zone increases landward and fluctuates in the surf

and swash zones, depending on the presence of a bar or a terrace that increases the local fluid

velocity.

Second, the spatial variation of the degree of sediment suspension is estimated using the

experimental finding of Kobayashi et al. (2005) who showed that the turbulent velocities

measured in the vicinity of the bottom were related to the energy dissipation rate due to bottom

friction. Representing the magnitude of the instantaneous turbulent velocity by $(D_f'/\rho)^{1/3}$ with

$D_f' = 0.5 \ \rho f_b \ U_a^3$ in light of Eq. (39), the probability P_s of sediment suspension is assumed to be

the same as the probability of $(D_f'/\rho)^{1/3}$ exceeding the sediment fall velocity w_f. The probability

P_s is then equal to the probability of $(r - r_m)^2 > F_s^2 = (R_s^2 - F_m^2)$ with $R_s = [(2/f_b)^{1/3} w_f/\sigma_T]$ and is

given by

$$P_s = \frac{1}{2} erfc\left(\frac{F_s - r_m}{\sqrt{2}}\right) + \frac{1}{2} erfc\left(\frac{F_s + r_m}{\sqrt{2}}\right) \quad \text{for} \quad F_s^2 > 0 \qquad (50)$$

and $P_s = 1$ for $F_s^2 \leq 0$. If $P_s > P_b$, use is made of $P_s = P_b$ assuming that sediment suspension occurs only when sediment movement occurs. Fine sands on beaches tend to be suspended once their movement is initiated.

Third, the suspended sediment volume V_s per unit horizontal bottom area is estimated by modifying the sediment suspension model by Kobayashi and Johnson (2001)

$$V_s = P_s \frac{e_B D_r + e_f D_f}{\rho g (s-1) w_f} \left(1+S_{bx}^2\right)^{0.5} \left(1+S_{by}^2\right)^{0.5} \quad ; \quad S_{bx} = \frac{\partial z_b}{\partial x} \quad ; \quad S_{by} = \frac{\partial z_b}{\partial y} \tag{51}$$

where S_{bx} = cross-shore bottom slope; S_{by} = longshore bottom slope; and e_B and e_f = suspension efficiencies for the energy dissipation rates D_r and D_f due to wave breaking and bottom friction, respectively. Use has been made of $e_B = 0.005$ and $e_f = 0.01$ as typical values in the computation of berm and dune erosion but the value of e_B is uncertain and should be calibrated if V_s is measured (Kobayashi et al. 2007a). The sediment suspension probability P_s is added in Eq. (51) to ensure $V_s = 0$ if $P_s = 0$. The term involving S_{bx} and S_{by} is the actual bottom area per unit horizontal bottom area and essentially unity except for very steep slopes. For the case of alongshore uniformity, $S_{by} = 0$. The cross-shore and longshore suspended sediment transport rates q_{sx} and q_{sy} are expressed as

$$q_{sx} = a_x \overline{U} V_s \quad ; \quad q_{sy} = \overline{V} V_s \quad ; \quad a_x = \left[a + \left(S_{bx} / \tan\phi\right)^{0.5} \right] \geq a \tag{52}$$

where a = empirical suspended load parameter and ϕ = angle of internal friction of the sediment with $\tan\phi = 0.63$ for sand (Bailard 1981). The parameter a accounts for the onshore suspended sediment transport due to the positive correlation between the time-varying cross-shore velocity and suspended sediment concentration. The value of a increases to unity as the positive correlation decreases to zero. For the three small-scale equilibrium profile tests conducted by

31

Kobayashi et al. (2005), *a* was of the order of 0.2. The effect of the cross-shore bottom slope on a_x was included by Kobayashi et al. (2009b) to increase berm and dune erosion. For $S_{bx} \le 0$, $a_x = a$. The cross-shore suspended sediment transport rate q_{sx} is negative (offshore) because the return (undertow) current $\overline{U}$ is negative (offshore). On the other hand, the longshore suspended sediment transport rate q_{sy} in Eq. (52) neglects the correlation between the time-varying longshore velocity and suspended sediment concentration, which appears to be very small if the longshore current $\overline{V}$ is sufficiently large. Payo et al. (2009) verified Eq. (52) using velocities and sand concentrations measured along 20 transects at the Field Research Facility at Duck, North Carolina during a storm in 1997.

Fourth, the formulas for the cross-shore and longshore bedload transport rates q_{bx} and q_{by} are devised somewhat intuitively because bedload in the surf zone has never been measured. The time-averaged rates q_{bx} and q_{by} are tentatively expressed as

$$q_{bx} = B_b \overline{(U^2 + V^2)U} \quad ; \quad q_{by} = B_b \overline{(U^2 + V^2)V} \tag{53}$$

where B_b = empirical parameter. Eq. (53) may be regarded as a quasi-steady application of the formula of Meyer-Peter and Mueller (e.g., Ribberink 1998). Substitution of U and V given in Eq. (27) with Eqs. (28) and (29) into Eq. (53) yields

$$q_{bx} = B_b \sigma_T^3 \left(b_* + U_* V_*^2 + 2F_m \sin\theta \right) \tag{54}$$

$$q_{by} = B_b \sigma_T^3 \left[V_* \left(1 + U_*^2 + V_*^2\right) - 2r_m \sin\theta \right] \tag{55}$$

where $b_* = \left(3U_* + U_*^3 \right)$ and F_m and r_m are defined in Eq. (44).

Eqs. (54) and (55) yield $q_{bx} = b_* B \sigma_T^3$ and $q_{by} = 0$ for normally incident waves with $\sin\theta = 0$ and

$V_* = 0$. The expressions of B_b and b_* are obtained by requiring that $q_{bx} = b_* B \sigma_T^3$ reduces to the

onshore bedload formula proposed by Kobayashi et al. (2008a) for normally incident waves,

which synthesized existing data and simple formulas. The proposed formulas are written as

$$q_{bx} = \frac{bP_b}{g(s-1)} \sigma_T^3 \left(1 + U_* V_*^2 + 2F_m \sin\theta\right) G_s\left(S_{bx}\right) \tag{56}$$

$$q_{by} = \frac{bP_b}{g(s-1)} \sigma_T^3 \left[V_* \left(1 + U_*^2 + V_*^2\right) - 2r_m \sin\theta\right] G_s\left(S_{by}\right) \tag{57}$$

where b = empirical bedload parameter; and G_s = bottom slope function. The sediment

movement probability P_b given in Eq. (49) accounts for the initiation of sediment movement. It

is noted that $b_* = 1$ in Eq. (56) to compensate for the limitations of Eq. (53) and the Gaussian

distribution of the horizontal velocity used in Eqs. (28) and (29) as discussed by Kobayashi et al.

(2008a). They calibrated $b = 0.002$ using the 20 water tunnel tests of Ribberink and Al-Salem

(1994), the 4 large-scale wave flume tests of Dohmen-Janssen and Hanes (2002), and the 24

sheet flow tests by Dohmen-Janssen et al. (2002). Furthermore, this simple bedload formula is

consistent with the sheet flow model for onshore bar migration by Trowbridge and Young (1989)

and the energetics-based bedload formula for steady flow by Bagnolds (1966) if the steady flow

formula is applied in the time-averaged manner. The onshore bedload transport predicted by Eq.

(56) is consistent with the field observations of onshore ripple migration by Becker et al. (2007)

and Masselink et al. (2007). The offshore suspended sediment transport predicted by Eq. (52) is

consistent with the field measurement during a storm by Madsen et al. (1994). The condition of

$\left(q_{bx} + q_{sx}\right) = 0$ for an equilibrium profile along with additional assumptions can be shown to

yield the equilibrium profile popularized by Dean (1991).

The bottom slope function $G_s(S_{bx})$ was introduced by Kobayashi et al. (2008a) to account for the effect of the steep cross-shore slope S_{bx} on the bedload transport rate and is expressed as

$$G_s(S_{bx}) = \tan\phi / (\tan\phi + S_{bx}) \qquad \text{for} \qquad -\tan\phi < S_{bx} < 0 \qquad (58)$$

$$G_s(S_{bx}) = (\tan\phi - 2S_{bx}) / (\tan\phi - S_{bx}) \qquad \text{for} \qquad 0 < S_{bx} < \tan\phi \qquad (59)$$

where $G_s = 1$ for $S_{bx} = 0$. Eq. (58) corresponds to the functional form of G_s used by Bagnold (1966) for steady stream flow on a downward slope with $S_{bx} < 0$ where the downward slope increases q_{bx}. Eq. (59) ensures that G_s approaches negative infinity as the upward slope S_{bx} approaches $\tan\phi$. Eqs. (58) and (59) reduce to $G_s = (1 - S_{bx} / \tan\phi)$ for $|S_{bx}| \ll \tan\phi$. Eq. (56) with G_s given by Eqs. (58) and (59) implies that the bedload transport rate q_{bx} is positive (onshore) for $S_{bx} < (\tan\phi)/2$ and negative (offshore) for $S_{bx} > (\tan\phi)/2$. Use is made of $|G_s| < G_m = 10$ to avoid an infinite value in the computation. The computed profile change is not very sensitive to the assumed value of G_m because the beach profile changes in such a way to reduce a very steep slope except in the region of scarping (e.g., Seymour et al. 2005). The effect of the longshore bottom slope S_{by} is included in Eq. (57) using the same bottom slope function $G_s(S_{by})$ but has never been validated for lack of suitable data.

The landward marching computation of the time-averaged model in the wet zone ends at the cross-shore location $x = x_r$ where the mean water depth $\overline{h}$ is less than 1 cm. No reliable data exists for suspended sand and bedload transport rates in the zone which is wet and dry intermittently. In the absence of wave overtopping [$q_o = 0$ in Eq. (19)], the following simple procedure was proposed by Kobayashi et al. (2008a) to deal with the zone with the bottom slope $S_{bx} > \tan\phi$. The cross-shore total sediment transport rate $q_x = (q_{sx} + q_{bx})$ at $x = x_r$ is denoted by

34

q_{xr}. If q_{xr} is negative (offshore), q_x is extrapolated linearly to estimate q_x on the scarped face with

$S_{bx} > \tan \phi$

$$q_x = q_{xr}(x_e - x)/(x_e - x_r) \quad \text{for} \quad x_r < x < x_e \tag{60}$$

where x_e = landward limit of the scarping zone with $S_{bx} > \tan \phi$. The extrapolated q_x is in the range of $q_{xr} \leq q_x \leq 0$ and the scarping zone is eroded due to the offshore sediment transport. This simple procedure is effective for a high and wide dune, that is typical in the Netherlands (e.g., van Gent et al. 2006), but does not allow onshore sediment transport due to overwash. The model for the wet and dry zone in Section 8 has been developed to predict wave overtopping and overwash of dunes.

Finally, the beach profile change is computed using the continuity equation of bottom sediment

$$\left(1 - n_p\right)\frac{\partial z_b}{\partial t} + \frac{\partial q_x}{\partial x} + \frac{\partial q_y}{\partial y} = 0 \tag{61}$$

where n_p = porosity of the bottom sediment which is normally taken as n_p = 0.4; t = slow morphological time for the change of the bottom elevation z_b; and $q_y = (q_{sy} + q_{by})$ = longshore total sediment transport rate. For the case of alongshore uniformity, the third term in Eq. (61) is zero. Eq. (61) is solved using an explicit Lax-Wendroff numerical scheme (e.g., Nairn and Southgate 1993) to obtain the bottom elevation at the next time level. This computation procedure is repeated starting from the initial bottom profile until the end of a profile evolution test. The computation time is of the order of 10^{-3} of the test duration.

6. Permeable Layer Model in Wet Zone

The combined wave and current model CSHORE has been extended to allow the presence of a permeable layer in the wet zone. Fig. 2 shows an example of irregular wave overtopping of a permeable slope where x = onshore coordinate: z = vertical coordinate, $\bar{\eta}$ = mean free surface elevation above SWL; S = storm tide above $z = 0$; z_b = bottom elevation; $\bar{h}$ = mean water depth; U = instantaneous depth-averaged cross-shore velocity above the bottom; z_p = elevation of the lower boundary of the permeable layer; $h_p = (z_b - z_p)$ = vertical thickness of the permeable layer; and U_p = instantaneous cross-shore discharge velocity inside the permeable layer. The cross-shore profiles of $z_b(x)$ and $z_p(x)$ are specified as input where $h_p = 0$ in the zone of no permeable layer. The lower boundary located at $z = z_p$ is assumed to be impermeable for simplicity. Kobayashi et al. (2007b) developed a permeable layer model in the wet zone for normally incident waves. This model is extended to obliquely incident waves in the following but the extended model has not been verified yet.
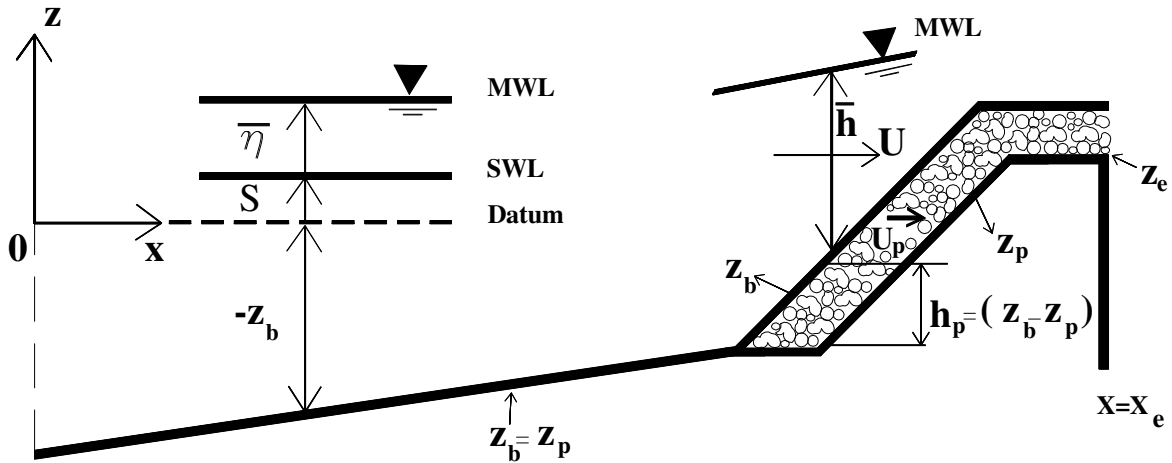

Fig. 2. Definition sketch of permeable layer model.

The time-dependent model for the flow over a permeable layer in shallow water developed by Kobayashi and Wurjanto (1990) and Wurjanto and Kobayashi (1993) is time-averaged and simplified to account for the permeable layer in the cross-shore model CSHORE. The vertically-integrated continuity equation (19) is modified as

$$Q_x = \overline{h}\,\overline{U} + \frac{g\sigma_\eta^2}{C}\cos\theta + q_r\cos\theta \quad ; \quad Q_x + h_p\overline{U_p} = q_o \tag{62}$$

where $\overline{U_p}$ = time-averaged cross-shore discharge velocity; $\left(h_p\overline{U_p}\right)$ = water flux inside the permeable layer with its vertical thickness h_p; and q_o = combined wave overtopping rate above and through the permeable layer. The cross-shore and longshore momentum equations (22) and (23) are assumed to remain the same, neglecting the momentum fluxes into and out of the permeable layer in the wet zone which is saturated with water. The bottom friction factor f_b for τ_{bx} and τ_{by} given by Eq. (33) includes the effect of the surface roughness of the permeable layer and was calibrated in the range of f_b = 0.01 – 0.05 (Kobayashi et al. 2007b). For the case of alongshore uniformity and negligible momentum fluxes into and out of the permeable layer in the wet zone, the time-averaged longshore discharge velocity $\overline{V_p}$ is assumed to be zero because of no or negligible driving force to cause the longshore discharge inside the permeable layer. It is noted that the assumption of $\overline{V_p} = 0$ cannot be validated at present for lack of suitable data.

On the other hand, the wave action equation (36) is modified as

$$\frac{d}{dx}\left[\frac{E}{\omega}\left(C_g\cos\theta + \frac{Q_x}{\overline{h}}\right)\right] = -\frac{D_B + D_f + D_p}{\omega} \tag{63}$$

where D_p = energy dissipation rate due to flow resistance in the permeable layer, assuming that the energy influx into the permeable layer equals the dissipation rate D_p per unit horizontal area. The dissipation rate D_p is expressed as (Wurjanto and Kobayashi 1993)

$$D_p = \rho h_p \left[\alpha_p \left(\overline{U_p^2 + V_p^2} \right) + \beta_p \left(\overline{U_p^2 + V_p^2} \right)^{1.5} \right] \tag{64}$$

where α_p and β_p = laminar and turbulent flow resistance coefficients, respectively, and V_p = instantaneous longshore discharge velocity. Kobayashi et al. (2007b) modified the formulas for α_p and β_p proposed by van Gent (1995) as follows:

$$\alpha_p = \alpha_0 \frac{\left(1 - n_p\right)^2}{n_p^2} \frac{\nu}{D_{n50}^2} \quad ; \quad \beta_p = \beta_1 + \frac{\beta_2}{\sigma_p} \tag{65}$$

with

$$\beta_1 = \frac{\beta_0 \left(1 - n_p\right)}{n_p^3 D_{n50}} \quad ; \quad \beta_2 = \frac{7.5 \beta_0 \left(1 - n_p\right)}{\sqrt{2}\, n_p^2 T} \tag{66}$$

where α_0 and β_0 = empirical parameters calibrated as α_0 = 1,000 and β_0 = 5; n_p = porosity of the permeable layer consisting of stone; ν = kinematic viscosity of the fluid; D_{n50} = nominal stone diameter defined as $D_{n50} = \left(M_{50} / \rho_s\right)^{1/3}$ with M_{50} = median stone mass and ρ_s = stone density; σ_p = standard deviation of the instantaneous discharge velocity; and T = intrinsic wave period used in Eq. (38).

The discharge velocities U_p and V_p in Eq. (64) are assumed to be expressed as

$$U_p = \overline{U_p} + r \sigma_p \cos\theta \quad ; \quad V_p = r \sigma_p \sin\theta \tag{67}$$

where r = Gaussian variable whose probability density function is given by Eq. (29); and θ = incident wave angle for the oscillatory velocity direction above and inside the permeable layer. The assumptions of the Gaussian velocity distribution and $\overline{V}_p = 0$ allow one to represent the discharge velocities by the mean cross-shore discharge velocity $\overline{U}_p$ and the standard deviation σ_p. Substitution of Eq. (67) into Eq. (64) yields

$$D_p = \rho h_p \left\{ \alpha_p \left(\overline{U}_p^{\,2} + \sigma_p^2 \right) + \sqrt{\frac{2}{\pi}} \left(\beta_2 + \beta_1 \sigma_p \right) \left[2\sigma_p^2 + \overline{U}_p^{\,2} \left(1 + 2\cos^2 \theta \right) \right] \right\} \tag{68}$$

where use is made of the approximate expression of G_f given by Eq. (48) and the assumption of $\left| \overline{U}_p \sin\theta \right| \ll \sigma_p$ to simplify Eq. (68). Approximate equations for $\overline{U}_p$ and σ_p are derived in the following.

Neglecting the inertia terms in the cross-shore momentum equation for the flow inside the permeable layer (Kobayashi and Wurjanto 1990), the local force balance between the cross-shore hydrostatic pressure gradient and flow resistance is assumed

$$g \frac{\partial \eta}{\partial x} + \alpha_p U_p + \beta_p U_p \left(U_p^2 + V_p^2 \right)^{0.5} = 0 \tag{69}$$

Eq. (69) is averaged probabilistically using Eq. (67). For the case of alongshore uniformity, the averaged force balance equation is expressed as

$$g \frac{d\overline{\eta}}{dx} + \overline{U}_p \left[\alpha_p + \sqrt{\frac{2}{\pi}} \left(\beta_2 + \beta_1 \sigma_p \right) \left(1 + \cos^2 \theta \right) \right] = 0 \tag{70}$$

where use is made of the approximate expression of G_{bx} given by Eq. (46) and the assumption of $\left| \overline{U}_p \sin\theta \right| \ll \sigma_p$ to simplify Eq. (70). It is noted that the local force balance between the

longshore hydrostatic pressure gradient and flow resistance yields $\overline{V}_p = 0$ for the case of alongshore uniformity where $\overline{\eta}$ is independent of the longshore coordinate y. To derive an equation σ_p, the approximate analytical method used by Kobayashi et al. (2007b) is adopted. Eq. (69) is linearized as

$$g\frac{\partial \eta}{\partial x} + \left(\alpha_p + 1.9\beta_p\sigma_p\right)U_p = 0 \tag{71}$$

which is used to obtain

$$\left[\alpha_p + 1.9\left(\beta_2 + \beta_1\sigma_p\right)\right]\sigma_p = gk\overline{h}\sigma_* \quad ; \quad \sigma_* = \sigma_\eta / \overline{h} \tag{72}$$

where the wave number k is computed using Eq. (2). Eq. (72) can be solved analytically to obtain σ_p for known $k\overline{h}\sigma_*$. After σ_p is obtained, Eq. (70) is used to calculate $\overline{U}_p$ for known $d\overline{\eta}/dx$. The energy dissipation rate D_p is computed using Eq. (68). Eq. (62) for assumed q_o is used to obtain Q_x and $\overline{U}$ where $\overline{U}$ is expressed by Eq. (42).

7. Irregular Wave Runup and Overtopping

The time-averaged model CSHORE in the wet zone does not predict the shoreline oscillations on beaches and coastal structures unlike time-dependent models (e.g., Wurjanto and Kobayashi 1993). Kobayashi et al. (2008b) proposed a probabilistic model for irregular wave runup as illustrated in Fig. 3. The shoreline oscillation is assumed to be measured by a runup wire (RW) placed parallel to the bottom elevation z_b at a vertical height of δ_r. The runup wire measures the instantaneous elevation η_r above SWL of the intersection between the wire and the free surface elevation. The mean $\overline{\eta}_r$ and standard deviation σ_r of η_r are estimated using the computed cross-

shore variations of $\bar{\eta}(x)$ and $\sigma_\eta(x)$ of the free surface elevation η above SWL. The

probabilities of η_r exceeding $(\bar{\eta}_r + \sigma_r)$, $\bar{\eta}_r$, and $(\bar{\eta}_r - \sigma_r)$ are assumed to be the same as the

probabilities of η exceeding $(\bar{\eta} + \sigma_\eta)$, $\bar{\eta}$, and $(\bar{\eta} - \sigma_\eta)$, respectively. The elevations of Z_1, Z_2,

and Z_3 of the intersections of $(\bar{\eta} + \sigma_\eta)$, $\bar{\eta}$, and $(\bar{\eta} - \sigma_\eta)$ with the runup wire are obtained for the

given wire elevation $(z_b + \delta_r)$. The obtained elevations are assumed to correspond to

$Z_1 = \left[\bar{\eta}_r + \sigma_r\right]$, $Z_2 = \bar{\eta}_r$, and $Z_3 = (\bar{\eta}_r - \sigma_r)$. The mean and standard deviation of η_r are

estimated as

$$\bar{\eta}_r = (Z_1 + Z_2 + Z_3)/3 \qquad ; \qquad \sigma_r = (Z_1 - Z_3)/2 \qquad (73)$$

In CSHORE2009, $\bar{\eta}$ and σ_η are replaced by $(P_w \bar{h} + z_b)$ and $P_w \sigma_\eta$ for the computation of Z_1, Z_2

and Z_3 to account for the transition from the wet zone ($P_w = 1$) to the wet and dry zone ($P_w < 1$)

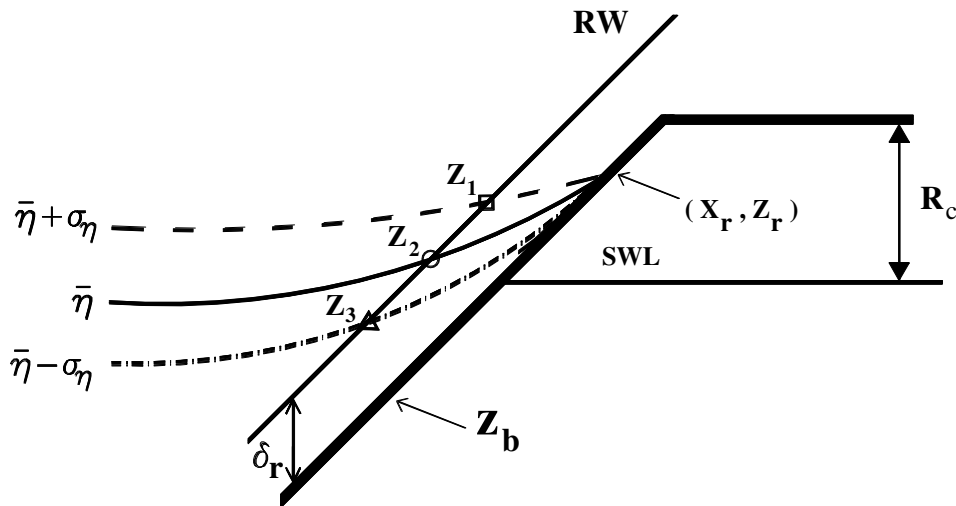where P_w is the wet probability explained in Section 8.

Fig. 3. Definition sketch for probabilistic model for irregular wave runup.

The runup height R is defined as the crest height above SWL of the temporal variation of η_r. The probability distribution of linear wave crests above the mean water level (MWL) is normally given by the Rayleigh distribution. For the case of no wave overtopping, the runup height $\left(R - \overline{\eta}_r\right)$ above the mean elevation $\overline{\eta}_r$ is assumed to be given by the Rayleigh distribution (Kobayashi et al. 2008b)

$$P(R) = \exp\left[-2\left(\frac{R - \overline{\eta}_r}{R_{1/3} - \overline{\eta}_r}\right)\right] \tag{74}$$

where $P(R)$ = exceedance probability of the runup height R above SWL; and $R_{1/3}$ = significant runup height defined as the average of 1/3 highest values of R. The mean $\overline{\eta}_r$ related to wave setup is normally neglected in Eq. (74) for the prediction of irregular wave runup on steep coastal structures. For the 1/5 and 1/2 permeable slope experiments conducted by Kobayashi et al. (2008b), $R_{1/3}$ was estimated as

$$R_{1/3} = \overline{\eta}_r + (2 + \tan\theta)\sigma_r \tag{75}$$

where θ = seaward slope angle from the horizontal and $\tan\theta = 1/5$ and 1/2 in the experiments. It is cautioned that Eqs. (74) and (75) have been calibrated only for permeable slopes with $\tan\theta$ = 0.2 – 0.5 in the absence of wave overtopping.

Wave overtopping occurs when the individual runup height R above SWL exceeds the structure crest height R_c above SWL as depicted in Fig. 3. Wave overtopping reduces R exceeding R_c because of overtopping flow on the crest. Kobayashi and de los Santos (2007) adopted the following Weibull distribution:

$$P(R) = \exp\left[-2\left(\frac{R - \overline{\eta}_r}{R_{1/3} - \overline{\eta}_r}\right)^{\kappa}\right] \tag{76}$$

with

$$\kappa = 2 + 0.5 R_*^{-3} \quad ; \quad R_* = \left(R_c - \overline{\eta}_r\right) / \left(R_{1/3} - \overline{\eta}_r\right) \tag{77}$$

where κ = shape parameter with $\kappa = 2$ for the Rayleigh distribution given by Eq. (74); and R_* = normalized crest height related to the wave overtopping probability P_o. The probability P_o of R exceeding R_c in Eq. (76) is given by

$$P_o = \exp\left(-2R_*^{\kappa}\right) \tag{78}$$

It should be noted that the empirical formula for κ given by Eq. (77) has been calibrated using only 22 permeable slope tests. The formula for $R_{1/3}$ given by Eq. (75) has been found to be applicable to these 22 tests. The runup height $R_{2\%}$ for the 2% exceedance probability obtained using Eq. (76) is given by

$$R_{2\%} = \overline{\eta}_r + (1.40)^{2/\kappa}\left(R_{1/3} - \overline{\eta}_r\right) \tag{79}$$

where the shape parameter κ given by Eq. (77) accounts for the decrease of $R_{2\%}$ due to the decrease of the normalized crest height R_* and the resulting increase of the wave overtopping probability P_o given by Eq. (78).

The wave overtopping rate q_o in Eq. (19) for an impermeable slope and in Eq. (62) for a permeable slope needs to be estimated if wave overtopping occurs at the landward end of the computation domain located at $x = x_e$ in Fig. 2. For permeable slopes, Kobayashi and de los Santos (2007) proposed the following empirical formula:

$$q_o = a_*\left(P_o\right)^{b_*} q_{SWL} + q_s \tag{80}$$

43

with

$$q_{SWL} = \frac{g\sigma_\eta^2}{C}\cos\theta \quad \text{at} \quad x = x_{SWL} \tag{81}$$

where a_* and b_* = empirical parameters; P_o = wave overtopping probability; q_{SWL} = wave-induced onshore flux in Eq. (62) evaluated at the still water shoreline located at $x = x_{SWL}$ with $z_b(x_{SWL}) = S$ in Fig. 2; and q_s = seepage rate through the permeable layer at $x = x_e$. It is noted that the roller effect has been neglected for relatively steep permeable slopes because of its negligible effect, probably because the roller does not develop over a relatively short distance on the steep slope. The empirical parameters a_* and b_* are assumed to depend on the horizontal width L_h of the permeable surface above the upper limit of wave setup located at (x_r, z_r) in Fig. 3 where the infiltration of overtopped water is assumed to be vertical due to gravity. The empirical formulas based on 32 tests were expressed as

$$a_* = \exp(-0.1L_*) \quad ; \quad b_* = 1 + 0.1L_* \quad ; \quad L_* = L_h / D_{n50} \tag{82}$$

where L_* = infiltration width normalized by the nominal stone diameter D_{n50}, crudely representing the horizontal number of stones above the maximum wave setup.

On the other hand, Kobayashi and de los Santos (2007) estimated the seepage rate q_s for normally incident waves

$$q_s = 0.2(z_r - z_e)^{1.5}\left[\frac{g}{(x_e - x_r)\beta_1}\right]^{0.5} \quad \text{for} \quad z_r > z_e \tag{83}$$

where z_e = elevation of the landward end of the impermeable surface z_p as shown in Fig. 2; and β_1 = turbulent flow resistance coefficient defined in Eq. (66). To derive Eq. (83), the seepage

flow was assumed to be driven by the horizontal pressure gradient from the point (x_r, z_r) to the

point (x_e, z_e). Consequently, $q_s = 0$ if $z_r < z_e$. If $x_r = x_e$, the permeable layer is wet always

and $q_s = h_p \overline{U}_p$ at $x = x_e$ where the water flux $h_p \overline{U}_p$ in the permeable layer is included in the

continuity equation (62).

Kobayashi et al. (2007c) examined the transition from little wave overtopping to excessive wave

overtopping and overflow on an impermeable smooth levee with a seaward slope of 1/5 in wave-

flume experiments consisting of 107 tests. For the impermeable slope, Eqs. (75) and (77) for the

permeable slope had to be modified as

$$R_{1/3} = \overline{\eta}_r + 4\sigma_r \quad ; \quad \kappa = 2 \tag{84}$$

The wave overtopping probability P_o is given by Eq. (78) with $\kappa = 2$ where the normalized crest

height R_* above SWL is defined in Eq. (77) with $R_{1/3}$ given by Eq. (84). It is noted $P_o = 1$ if

$R_* < 0$. For the impermeable slope, the seepage rate $q_s = 0$ in Eq. (80) and Eq. (82) yields

$a_* = 1$ and $b_* = 1$ for $L_h = 0$. As a result, the wave overtopping rate q_o is given by $q_o = P_o q_{SWL}$.

For the case of combined wave overtopping and overflow, Kobayashi et al. (2007c) expressed

the combined rate q_o as

$$q_o = P_o q_{SWL} + H_{SWL} \sqrt{g H_{SWL}} \quad \text{for} \quad H_{SWL} > 0 \tag{85}$$

with

$$H_{SWL} = \overline{\eta} - R_c \quad \text{at} \quad x = x_{SWL} \tag{86}$$

where H_{SWL} = head for the overflow; $\overline{\eta}$ = mean water level above SWL; and R_c = levee crest

height above SWL. If $R_c < 0$, the levee crest is below SWL and x_{SWL} is chosen at the seaward

edge of the levee crest. For $H_{SWL} > 0$, H_{SWL} is the mean water level above the levee crest and $\sqrt{gH_{SWL}}$ may be regarded as the water velocity on the crest.

In summary, Eqs. (73) – (86) are essentially empirical and were used in the cross-shore model CSHORE2008 to predict irregular wave runup, overtopping, seepage and overflow on permeable and impermeable structures. These equations have not been verified for irregular wave overtopping and overflow of dunes. These equations do not predict the spatial variations of the hydrodynamic variables required for the sediment model and the computation of dune profile evolution. Consequently, a hydrodynamic model for the intermittently wet zone landward of the maximum wave setup has been developed in Section 8. In CSHORE2009, the formula for P_o given by Eq. (78) and the formulas for q_o given by Eqs. (80) and (85) are removed and replaced by new formulas for P_o and q_o based on the hydrodynamic model for the wet and dry zone. The values of $\overline{\eta}_r, \sigma_r, R_{1/3}$ and $R_{2\%}$ are computed in CSHORE2009 because this hydrodynamic model does not predict individual wave runup events.

8. Model for Impermeable Wet and Dry Zone

Time-dependent numerical models such as the nonlinear shallow-water wave model by Kobayashi et al. (1989) can predict the water depth and horizontal velocity in the intermittently wet and dry (swash) zone on beaches and inclined structures. However, the time-dependent hydrodynamic computation requires considerable computation time and may not lead to an accurate prediction of dune profile evolution in view of the earlier attempt by Tega and Kobayashi (1996). A time-averaged probabilistic model is developed here to predict the cross-

46

shore variations of the wet probability and the mean and standard deviation of the water depth and cross-shore velocity in the swash. The developed model is very efficient computationally and can be calibrated using a large number of data sets. The present model is limited to normally incident waves and alongshore uniformity. A sediment transport model in the swash zone is formulated by modifying the sediment transport model in the wet zone.

8.1 Water depth and velocity

Van Gent (2002a) and Schüttrumpf and Oumeraci (2005) analyzed the water depth and velocity of waves overtopping of dikes. Kobayashi et al. (2010) expanded their analyses for the prediction of wave overtopping and overwash as presented in the following.

For normally incident waves on impermeable beaches and inclined structures of alongshore uniformity, the time-averaged cross-shore continuity and momentum equations derived from the nonlinear shallow-water wave equations are expressed as

$$\overline{hU} = q_o \tag{87}$$

$$\frac{d}{dx}\left(\overline{hU^2} + \frac{g}{2}\overline{h^2}\right) = -gS_{bx}\overline{h} - \frac{1}{2}f_b\overline{|U|U} \quad ; \quad S_{bx} = \frac{dz_b}{dx} \tag{88}$$

where h and U = instantaneous water depth and cross-shore velocity, respectively; q_o = wave overtopping rate; g = gravitational acceleration; S_{bx} = cross-shore bottom slope; and f_b = bottom friction factor which is allowed to vary spatially. The wave energy equation corresponding to Eqs. (87) and (88) was given by Kobayashi and Wurjanto (1992) who used it to estimate the rate of wave energy dissipation due to wave breaking. The wave energy equation is

not used in CSHORE because no formula is available to estimate the time-averaged energy dissipation rate in the wet and dry zone.

The instantaneous water depth h depends on the cross-shore coordinate x and the swash hydrodynamic time t. The water depth h at given x is described probabilistically rather than in the time domain. Kobayashi et al. (1998) analyzed the probability distributions of the free surface elevations measured in the shoaling, surf and swash zones. The measured probability distributions were shown to be in agreement with the exponential gamma distribution which reduces to the Gaussian distribution and the exponential distribution when the skewness approaches zero offshore and two in the swash zone, respectively. The assumption for the Gaussian distribution assumed in Eq. (29) has simplified the cross-shore model CSHORE in the wet zone significantly. The assumption of the exponential distribution is made here to simplify the cross-shore model in the wet and dry zone. The probability density function $f(h)$ is expressed as

$$f(h) = \frac{P_w^2}{\bar{h}}\exp\left(-P_w\frac{h}{\bar{h}}\right) \quad \text{for} \quad h > 0 \tag{89}$$

with

$$P_w = \int_0^\infty f(h)\,dh \quad ; \quad \bar{h} = \int_0^\infty hf(h)\,dh \tag{90}$$

where P_w = wet probability for the water depth $h > 0$; and $\bar{h}$ = mean water depth for the wet duration. The dry probability of $h = 0$ is equal to $(1 - P_w)$. The mean water depth for the entire duration is equal to $P_w\bar{h}$. The overbar in Eqs. (87) and (88) indicates averaging for the wet

duration only. The free surface elevation $(\eta - \overline{\eta})$ above MWL is equal to $(h - \overline{h})$. The standard

deviations of η and h are the same and given by

$$\frac{\sigma_\eta}{\overline{h}} = \left(\frac{2}{P_w} - 2 + P_w \right)^{0.5} \tag{91}$$

which yields $\sigma_\eta = \overline{h}$ for $P_w = 1$. This equality was supported by the depth measurements in the

lower swash zone by Kobayashi et al. (1998) who assumed $P_w = 1$ in Eq. (89).

The cross-shore velocity U depends on x and t and is related to the depth h in the swash

zone. The following relationship between U and h may be assumed to express U as a function

of h

$$U = \alpha \sqrt{gh} + U_s \tag{92}$$

where α = positive constant exceeding unity for supercritical flow; and U_s = steady velocity

which is allowed to vary with x. The steady velocity U_s is intended to account for offshore

return flow on the seaward slope and the downward velocity increase on the landward slope.

Holland et al. (1991) measured the bore speed and flow depth on a barrier island using video

techniques and obtained $\alpha \simeq 2$ where the celerity and fluid velocity of the bore are assumed to

be approximately the same. Tega and Kobayashi (1996) computed wave overtopping of dunes

using the nonlinear shallow-water wave equations and showed $\alpha \simeq 2$ for the computed U and

h. As a result, use may be made of $\alpha = 2$ as a first approximation. Eq. (92) implies that the

cross-shore velocity U increases monotonically with the increase of h at given x. Eq. (92)

yields $U = U_s$ when $h = 0$, which may be acceptable in view of the very small depth in the wet

and dry zone. Using Eqs. (89) and (92), the mean $\overline{U}$ and standard deviation σ_U of the cross-shore velocity U can be expressed as

$$\overline{U} = \frac{\sqrt{\pi}}{2}\alpha\left(P_w g\overline{h}\right)^{0.5} + P_w U_s \tag{93}$$

$$\sigma_U^2 = \alpha^2 g\overline{h} - 2\left(\overline{U} - U_s\right)\left(\overline{U} - P_w U_s\right) + P_w\left(\overline{U} - U_s\right)^2 \tag{94}$$

Eq. (92) is substituted into Eqs. (87) and (88) which are averaged for the wet duration using Eq. (89). The continuity equation (87) yields

$$\frac{3\sqrt{\pi}\alpha}{4}\overline{h}\left(\frac{g\overline{h}}{P_w}\right)^{0.5} + U_s\overline{h} = q_o \tag{95}$$

After lengthy algebra, the cross-shore momentum equation (88) is expressed as

$$\frac{d}{dx}\left(B\frac{g\overline{h}^2}{P_w} + \frac{q_o^2}{\overline{h}}\right) = -gS_{bx}\overline{h} - \frac{f_b}{2}\alpha^2 g\overline{h}G_b\left(r_s\right) \tag{96}$$

with

$$B = \left(2 - \frac{9\pi}{16}\right)\alpha^2 + 1 \quad ; \quad r_s = \frac{3\sqrt{\pi}}{4}\frac{U_s\overline{h}}{q_o - U_s\overline{h}} \tag{97}$$

The function $G_b\left(r_s\right)$ in Eq. (96) with $r = r_s$ for simplicity is given by

$$G_b(r) = 1 + \sqrt{\pi}\,r + r^2 \qquad\qquad \text{for } r \geq 0 \tag{98}$$

$$G_b(r) = 2\exp\left(-r^2\right) - r^2 - 1 + \sqrt{\pi}\,r\left[2\,erf(r) + 1\right] \quad \text{for } r < 0 \tag{99}$$

where *erf* is the error function. The function G_b increases monotonically with the increase of r and $G_b = 0$ and 1 for $r = -0.94$ and 0.0, respectively, as shown in Fig. 4. For $r < -1.5$, $G_b \simeq -\left(1 + \sqrt{\pi}r + r^2\right)$.
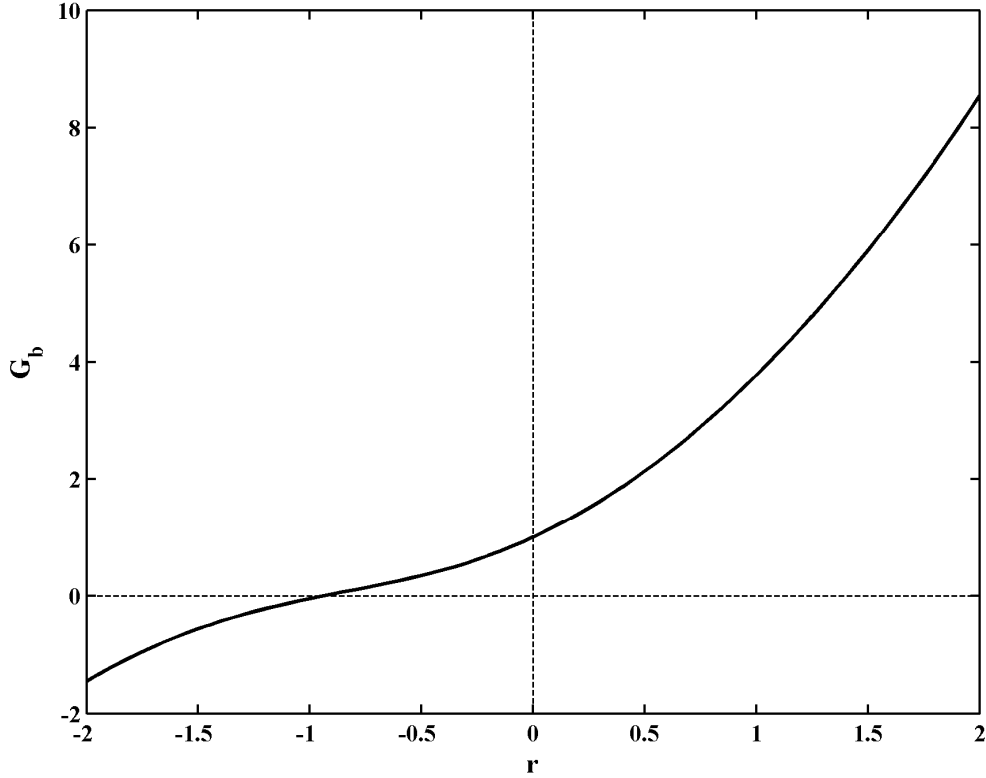

Fig. 4. Function $G_b(r)$ for wet and dry zone.

Eqs. (95) and (96) are used to predict the cross-shore variation of $\overline{h}$ and U_s for assumed q_o where $\sigma_\eta, \overline{U}$ and σ_U are computed using Eqs. (91), (93) and (94), respectively. It is necessary to estimate the wet probability P_w empirically. To simplify the integration of the momentum equation (96), the following formula is adopted:

51

$$P_w = \left[(1+A_o) \left(\frac{\bar{h}_1}{\bar{h}} \right)^n - A_o \left(\frac{\bar{h}_1}{\bar{h}} \right)^3 \right]^{-1} \quad ; \quad A_o = \frac{q_o^2}{Bg\bar{h}_1^{-3}} \quad \text{for} \quad x \le x_c \tag{100}$$

where $\bar{h}_1$ = mean water depth at the location of $P_w = 1$; n = empirical parameter for P_w; A_o = parameter related to the wave overtopping rate q_o normalized by the depth $\bar{h}_1$ where water is present always. The transition from the wet ($P_w = 1$ always) zone to the wet and dry ($P_w < 1$) zone may be taken at $x = x_{SWL}$ where x_{SWL} is the cross-shore location of the still water shoreline of an emerged slope (see Fig. 5) or the seaward edge of a submerged crest as discussed in relation to Eqs. (85) and (86). Eq. (100) is assumed to be valid on the seaward slope and crest in the region of $x \le x_c$ where x_c = landward end of the horizontal crest in Fig. 5.
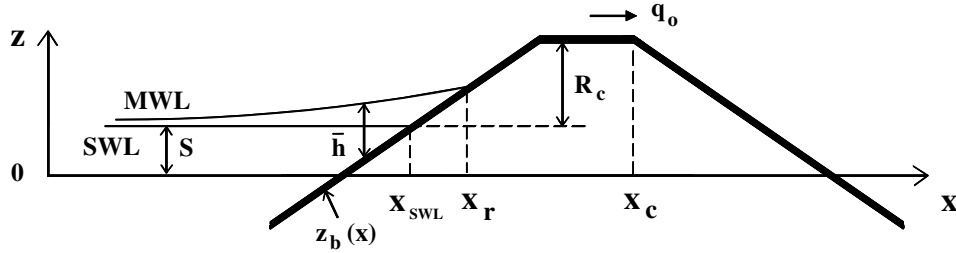

Fig. 5. Transition from wet model $(x < x_r)$ to wet and dry model $(x > x_{SWL})$ for emerged impermeable structure $(R_c > 0)$.

Integration of Eq. (96) for P_w given by Eq. (100) with $\bar{h} = \bar{h}_1$ at $x = x_1$ yields $\bar{h}(x)$ for $x_1 \le x \le x_c$

$$B_n (1+A_o) \bar{h}_1 \left[\left(\frac{\bar{h}_1}{\bar{h}} \right)^{n-1} - 1 \right] = z_b(x) - z_b(x_1) + \frac{\alpha^2}{2} \int_{x_1}^{x} f_b G_b dx \tag{101}$$

where $B_n = B(2-n)/(n-1)$; and $z_b(x)$ = bottom elevation at the cross-shore location x. The mean water depth $\bar{h}$ at given x is computed by solving Eq. (101) iteratively where the bottom

friction factor f_b is allowed to vary with x and the function G_b given by Eqs. (98) and (99) depends on r_s defined in Eq. (97). The empirical parameter n is taken to be in the range of $1 < n < 2$ so that $B_n > 0$. The formula for n calibrated using the 107 tests of wave overtopping and overflow on a dike by Farhadzadeh et al. (2007) was expressed as $n = 1.01 + 0.98\left[\tanh\left(A_o\right)\right]^{0.3}$ where $1.01 \le n \le 1.99$.

The wave overtopping and overflow rate q_o is predicted by imposing $U_s = 0$ in Eq. (95) at the location of x_c

$$q_o = \frac{3\sqrt{\pi}\alpha}{4}\bar{h}_c\left(\frac{g\bar{h}_c}{P_c}\right)^{0.5} \quad \text{at} \quad x = x_c \tag{102}$$

where $\bar{h}_c$ and P_c are the computed mean depth $\bar{h}$ and wet probability P_w at x_c. The wave overtopping probability P_o may be related to the wet probability P_c at $x = x_c$ where both P_o and P_c are in the range of 0.0 – 1.0. The empirical relation of $P_o = \left[\tanh(5P_c)\right]^{0.8}$ is fitted for the 107 tests by Farhadzadeh et al. (2007).

On the slope landward of the crest, the wet probability P_w is assumed to be constant and equal to P_c

$$P_w = P_c \quad \text{for} \quad x \ge x_c \tag{103}$$

Substituting Eq. (103) into Eq. (96) and integrating the resulting equation from x_c to x, the mean depth $\bar{h}(x)$ on the landward slope in the region of $x > x_c$ is expressed as

$$\frac{\bar{h}}{\bar{h}_c} - 1 + \frac{9\pi\alpha^2}{64B}\left[\left(\frac{\bar{h}_c}{\bar{h}}\right)^2 - 1\right] = \frac{P_c}{2B\bar{h}_c}\left[z_b(x_c) - z_b(x) - \frac{\alpha^2}{2}\int_{x_c}^{x} f_b G_b dx\right] \qquad (104)$$

where the bottom elevation $z_b(x)$ decreases with the landward increase of x in the region of

$x > x_c$. Eq. (104) is solved iteratively to compute $\bar{h}$ at given x.

For assumed q_o, the landward marching computation of $\bar{h}$, σ_η, $\bar{U}$ and σ_U is initiated using the

wet model in Section 4 from the seaward boundary $x = 0$ to the landward limit located at $x = x_r$

which corresponds to the location where the computed $\bar{h}$ or σ_η becomes negative or $\bar{h}$ becomes

less than 0.1 cm for an emerged crest as shown in Fig. 5. For a submerged crest, the landward

limit of x_r is taken as x_c. The landward marching computation is continued using the wet and

dry model in this section from the location of $x = x_{SWL}$ where $\bar{h} = \bar{h}_1$ in Eq. (101) to the landward

end of the computation domain or until the mean depth $\bar{h}$ becomes less than 0.001 cm. Then,

the rate q_o is computed using Eq. (102). This landward computation starting from $q_o = 0$ is

repeated until the difference between the computed and assumed values of q_o is less than 1%.

This convergency is normally obtained after several iterations. The computed values of $\bar{h}, \sigma_\eta, \bar{U}$

and σ_U by the two different models in the overlapping zone of $x_{SWL} < x < x_r$ (see Fig. 5) are

averaged to smooth the transition from the wet zone to the wet and dry zone.

Kobayashi et al. (2010) compared this hydrodynamic model for the impermeable wet and dry

zone with the 107 tests by Farhadzadeh et al. (2007) and the 100 tests conducted by van Gent

(2002b) who measured the water depth and velocities on the crest and landward (inner) slopes of

six different dikes. The agreement was mostly within a factor of two for the wave overtopping rates and probabilities as well as the water depth, velocity, and discharge on the crest and landward slope exceeded by 2% of the incident 1000 waves. Kobayashi et al. (2010) modified Eqs. (101) and (104) to allow the integration of Eq. (96) starting from an arbitrary location landward of the still water shoreline. This modification is necessary for a berm that is slanted downward toward the toe of a dune. The wet probability P_w on the downward berm slope is assumed to be the same as that at the seaward end of this downward slope in the same way as in Eq. (103) for the downward dune slope.

8.2 Sediment transport

The sediment transport model for the wet zone in Section 5 is adjusted for the wet and dry zone. Normally incident waves and alongshore uniformity are assumed here. The Gaussian velocity distribution has been assumed in Section 5, whereas U in the wet and dry zone is expressed as Eq. (92) along with the exponential distribution of h given by Eq. (89).

First, the movement of sediment particles is assumed to occur when the instantaneous bottom shear stress given by $0.5\rho f_b U^2$ exceeds the critical shear stress $\rho g (s-1) d_{50} \psi_c$ as has been assumed for Eq. (49). The probability P_b of sediment movement is then the same as the probability of $|U| > U_{cb}$ where $U_{cb} = \left[2g (s-1) d_{50} \psi_c f_b^{-1} \right]^{0.5}$. Using Eqs. (89) and (92), P_b can be shown to be given by

$$P_b = P_w \qquad\qquad \text{for } U_s > U_{cb} \qquad (105)$$

$$P_b = P_w \exp\left[-\frac{P_w \left(U_{cb} - U_s\right)^2}{\alpha^2 g \bar{h}} \right] \qquad\qquad \text{for } \left|U_s\right| \le U_{cb} \qquad (106)$$

$$P_b = P_w \left\{ 1 - \exp\left[-\frac{P_w \left(U_{cb} + U_s\right)^2}{\alpha^2 g \bar{h}} \right] + \exp\left[-\frac{P_w \left(U_{cb} - U_s\right)^2}{\alpha^2 g \bar{h}} \right] \right\} \qquad \text{for } -U_s > U_{cb} \qquad (107)$$

where the upper limit of P_b is the wet probability P_w because no sediment movement occurs during the dry duration.

Second, sediment suspension is assumed to occur when the instantaneous turbulent velocity estimated as $\left(f_b/2\right)^{1/3}\left|U\right|$ exceeds the sediment fall velocity w_f as has been assumed for Eq. (50). The probability P_s of sediment suspension is then the same as the probability of $\left|U\right| > U_{cs}$ where $U_{cs} = w_f\left(2/f_b\right)^{1/3}$. The probability P_s is then given by

$$P_s = P_w \qquad\qquad \text{for } U_s > U_{cs} \qquad (108)$$

$$P_s = P_w \exp\left[-\frac{P_w \left(U_{cs} - U_s\right)^2}{\alpha^2 g \bar{h}} \right] \qquad\qquad \text{for } \left|U_s\right| \le U_{cs} \qquad (109)$$

$$P_s = P_w \left\{ 1 - \exp\left[-\frac{P_w \left(U_{cs} + U_s\right)^2}{\alpha^2 g \bar{h}} \right] + \exp\left[-\frac{P_w \left(U_{cs} - U_s\right)^2}{\alpha^2 g \bar{h}} \right] \right\} \qquad \text{for } -U_s > U_{cs} \qquad (110)$$

which reduces to Eqs. (105) – (107) if U_{cs} is replaced by U_{cb}. If $P_s > P_b$, use is made of $P_s = P_b$ because sediment suspension occurs only when sediment movement occurs.

56

Third, the suspended sediment volume V_s per unit horizontal bottom area in the wet zone is estimated using Eq. (51) where $S_{by} = 0$ for alongshore uniformity. CSHORE2008 (Kobayashi and Farhadzadeh 2008) estimated V_s using the same equation with the assumption of negligible wave breaking in the wet and dry zone. This approach was unsuccessful. In the wet and dry zone, V_s is assumed in CSHORE2009 to be given by

$$V_s = P_s V_{Bf} \left(1 + S_{bx}^2\right)^{0.5} \tag{111}$$

where V_{Bf} = potential suspended sediment volume on a horizontal bottom when $P_s = 1$. The value of V_{Bf} is assumed to be constant and chosen so that the suspended sediment volume V_s is continuous at $x = x_{\mathrm{SWL}}$ at the seaward end of the wet and dry zone. The assumption of constant V_{Bf} may be reasonable because suspended sediment in the swash zone tends to remain suspended. It is noted that P_s given by Eqs. (108) – (110) decreases landward with the decrease of P_w

Kobayashi et al. (2010) estimated the cross-shore suspended sediment transport rate q_{sx} using Eq. (52).

$$q_{sx} = a_x \overline{U} V_s \quad ; \quad a_x = \left[a + \left(S_{bx} / \tan \phi\right)^{0.5}\right] \geq a \tag{112}$$

where $\overline{U}$ is given by Eq. (93). The parameter a_x had to be taken as unity in the zone of $\overline{U} > 0$ over the dune crest to predict minor wave overwash. However, Eq. (112) was found to underpredict major wave overwash in the three small-scale tests conducted by Figlus et al. (2009) to investigate the transition from minor to major wave overwash of dunes constructed of

fine sand. For these tests, suspended load was computed to be dominant. In order to account for the wave overtopping rate q_o explicitly, Eq. (112) is modified as

$$q_{sx} = \left(a_x \overline{U} + a_o U_o \right) V_s \quad ; \quad U_o = q_o / \overline{h} \tag{113}$$

where a_o = empirical parameter with $a_o = 0$ in Eq. (112); and U_o = onshore current due to q_o, which is significant only in the zone of the very small depth $\overline{h}$. The parameter a_x is the same as in Eq. (112) without any adjustment in the zone of $\overline{U} > 0$. The calibrated value for the three tests by Figlus et al. (2009) was in the range of $a_o = 1.3 - 1.8$. However, the range of $a_o = 0.1 -$ 0.5 was necessary for the minor wave overwash data used by Kobayashi et al. (2010) to calibrate Eqs. (111) and (112). The accurate prediction of wave overtopping and overwash is very difficult because of the small water depth and large velocity in the zone which is wet intermittently.

Fourth, the cross-shore bedload transport rate q_{bx} is estimated using Eq. (56) for the case of normally incident waves $\left(\sin \theta = 0 \right)$ and no longshore current $\left(\overline{V} = 0 \right)$ where $\sigma_T = \sigma_U$ for $\sin \theta = 0$ in Eq. (32). For this case, q_{bx} is given by

$$q_{bx} = \frac{b P_b \sigma_U^3}{g(s-1)} G_s \left(S_{bx} \right) \tag{114}$$

where the bottom slope function $G_s \left(S_{bx} \right)$ is given by Eqs. (58) and (59), and the standard deviation σ_U is given by Eq. (94) for the wet and dry zone. The parameter b in the wet and dry zone is chosen so that the value of q_b is continuous at $x = x_{SWL}$.

Finally, the cross-shore sediment transport rates q_{sx} and q_{bx} computed for the wet zone and the wet and dry zone are averaged in the overlapping zone of $x_{SWL} < x < x_r$ for the smooth transition between the two zones in the same way as the smooth transition of $\bar{h}, \sigma_\eta, \bar{U}$ and σ_U as explained at the end of Section 8.1. The linear extrapolation for the case of no overwash given by Eq. (60) for scarping is not applied now that the sediment transport in the wet and dry zone is predicted. The continuity equation of bottom sediment given by Eq. (61) with $q_y = 0$ is solved numerically to obtain the bottom elevation at the next time level.

9. Model for Permeable Wet and Dry Zone

The model in Section 8 is extended to a permeable wet and dry zone. The extended model is calibrated and verified using available data for stone structures.

A number of time-dependent hydrodynamic models for rubble mound structures have already been developed as reviewed by Losada et al. (2008). These numerical models try to predict the temporal and spatial variations of wave dynamics as accurately as possible. The computation time normally increases with the increase of the resolution and accuracy. The computationally advanced models are used to predict hydrodynamic variables for relatively short durations. To reduce computation time considerably, Kobayashi et al. (2007b) proposed the probabilistic model CSHORE. The time-varying wave variables are expressed using a probability distribution. The spatial variations of the mean and standard deviation are computed using the time-averaged governing equations. The probabilistic time-averaged model requires additional assumptions but its computational efficiency allows the calibration of the model parameters using a large number of tests. This probabilistic model for the wet zone on the permeable armor

59

layer is extended in this section to the wet and dry zone in order to predict the wave motion above the still water level (SWL). The extended model provides the hydrodynamic input to a damage progression model that predicts the slow evolution of the armor layer profile.

The movement of individual stone units on the armor layer may be computed using the equation of motion for each armor unit (Kobayashi and Otta 1987). The profile evolution of the armor layer may then be predicted by computing the displacements of all the armor units (Norton and Holmes 1992). However, this approach has never been adopted for practical applications probably because of its computation time. The sediment transport model in Section 8.2 is modified in this section to predict the profile evolution of the armor layer in the same manner as the prediction of the beach profile evolution. This simple approach neglects the discrete nature of armor stone units but is very convenient for the prediction of the armor layer profile evolution averaged alongshore where the alongshore averaging reduces the discrete nature.
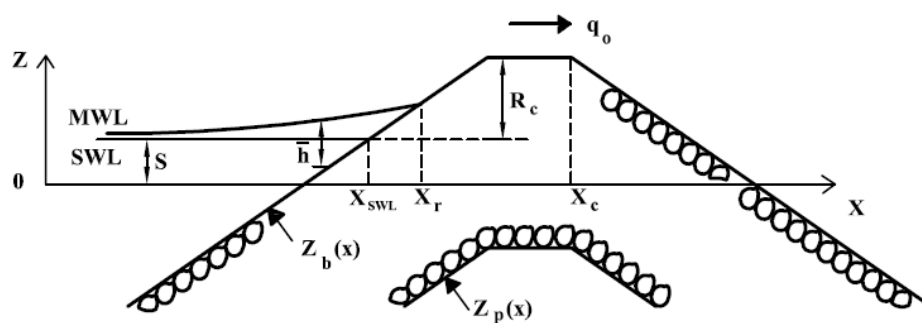

Fig. 6. Transition from wet model $(x < x_r)$ to wet and dry model $(x > x_{SWL})$ on permeable stone layer

9.1 Water depth and velocity

Fig. 6 depicts the permeable stone layer analyzed in this section. Alongshore uniformity and normally incident waves are assumed. The cross-shore coordinate x is positive onshore with $x=0$ at the offshore location of the wave measurement. The vertical coordinate z is positive upward with $z=0$ at the datum. The still water level (SWL) above the datum is allowed to vary in time during a storm or an experiment. The upper and lower boundaries of the permeable stone layer are located at $z = z_b(x)$ and $z_p(x)$, respectively, where the lower boundary is assumed to be impermeable to simplify the analysis. The crest height R_c is taken conventionally as the structure height above SWL. The crest location x_c is defined here as the highest and most landward location. The wave overtopping rate is denoted as q_o. The SWL shoreline on the seaward slope is located at x_{SWL}. The mean water level (MWL) is located at $z = \left(S + \overline{\eta} \right)$ where $\overline{\eta}$ is the wave setup above SWL. The mean water depth $\overline{h}$ above $z = z_b$ is given by $\overline{h} = \left(S + \overline{\eta} - z_b \right)$. The cross-shore location x_r is the landward limit of the time-averaged model in the wet zone presented in Section 6.

The time-averaged model for the permeable slope developed by Kobayashi et al. (2007b) has been modified using linear wave and current theory where wave overtopping induces onshore current. The time-averaged continuity, momentum, and wave action equations are used to predict the cross-shore variations of the mean $\overline{U}$ of the depth-averaged cross-shore velocity U, the mean $\overline{\eta}$ of the free surface elevation η above SWL, and the free surface standard deviation σ_η. The overbar denotes time averaging. The root-mean-square (RMS) wave height is defined as $H_{rms} = \sqrt{8}\,\sigma_\eta$. Linear progressive wave theory is used locally to express the velocity standard

deviation σ_U in terms of σ_η. The probability distributions of η and U are assumed to be Gaussian. The equivalency of the time averaging and probabilistic averaging is assumed to express the time-averaged terms in the governing equations in terms of $\overline{\eta}$, σ_η, $\overline{U}$ and σ_U. The permeability effects are included in the Section 6.

The landward-marching computation using this model for the wet zone is continued as long as the computed $\overline{h}$ and σ_η are larger than 0.1 cm. The end location of the computation is denoted as x_r in Fig. 6. The time-average model for the wet zone cannot predict wave overtopping. Consequently, CSHORE2008 relied on empirical formulas for wave overtopping and seepage rates. A separate model for the wet and dry zone is developed and connected with the model for the wet zone. This procedure is the same as that used in Section 8.1. The time-averaged cross-shore continuity and momentum equations derived from the nonlinear shallow-water wave equations on the permeable slope (Wurjanto and Kobayashi 1993) are expressed as

$$\frac{d}{dx}\left(\overline{hU}\right) = -\overline{w}_p \tag{115}$$

$$\frac{d}{dx}\left(\overline{hU^2} + \frac{g}{2}\overline{h^2}\right) = -g\overline{h}\frac{dz_b}{dx} - \frac{1}{2}f_b\overline{U|U|} - \overline{u_b w_p} \tag{116}$$

where h and U = instantaneous water depth and cross-shore velocity, respectively; w_p = vertical seepage velocity which is taken to be positive downward; g = gravitational acceleration; z_b = bottom elevation above the datum $z=0$; f_b = bottom friction factor which is allowed to vary spatially; and u_b = horizontal fluid velocity at $z = z_b$. The last term on the right hand side of Eq. (116) represents the time-averaged flux of the horizontal momentum into the permeable layer.

The overbar in Eqs. (115) and (116) for the wet and dry zone indicates averaging for the wet duration only because no water exists during the dry duration.

The continuity and approximate momentum equations for the flow inside the permeable layer are expressed as

$$\frac{dq_p}{dx} = \overline{w_p} \tag{117}$$

$$\left(\alpha_p + \beta_1 \left|\overline{U_p}\right|\right)\overline{U_p} = -g\frac{d\overline{\eta}}{dx} \tag{118}$$

with

$$\alpha_p = 1000\left(\frac{1-n_p}{n_p}\right)^2 \frac{\nu}{D_{n50}^2} \quad ; \quad \beta_1 = \frac{5(1-n_p)}{D_{n50}n_p^3} \tag{119}$$

where q_p = time-averaged horizontal volume flux in the permeable layer; $\overline{U_p}$ = time-averaged horizontal discharge velocity; α_p and β_1 = coefficients associated with the laminar and turbulent flow resistance in Eq. (65), respectively; n_p = porosity of the permeable layer; D_{n50} = nominal stone diameter; and ν = kinetic viscosity of the fluid. Eq. (119) is based on the formula developed by van Gent (1995) and calibrated by Kobayashi et al. (2007b). The resistance component associated with the oscillatory flow is simply neglected in Eq. (118) which is solved analytically to obtain the discharge velocity $\overline{U_p}$ driven by the horizontal pressure gradient due to $\overline{\eta} = \left(\overline{h} + z_b - S\right)$ where $\overline{h}$ and z_b vary with x. It is noted that Eq. (118) retains only the leading terms in the horizontal momentum equation given by Wurjanto and Kobayashi (1993).

Adding Eqs. (115) and (117) and integrating the resulting equation with respect to x, the vertically integrated continuity equation is obtained

$$\overline{hU} + q_p = q_o \tag{120}$$

where the wave overtopping rate q_o is defined as the sum of the volume fluxes above and inside the permeable layer in the same way as in Eq. (62). The volume flux q_p is estimated as

$$q_p = P_w \overline{U}_p \left(\overline{\eta}_p - z_p \right) \tag{121}$$

where P_w = wet probability defined as the ratio between the wet and entire durations: $\overline{\eta}_p$ = average water level inside the permeable layer; and z_p = elevation of the impermeable lower boundary. The elevation $\overline{\eta}_p$ and z_p are relative to the datum $z = 0$ in Fig. 6 and $\left(\overline{\eta}_p - z_p \right)$ is the thickness of water inside the permeable layer. The elevation $\overline{\eta}_p$ is estimated as

$$\overline{\eta}_p = P_w z_b + (1 - P_w) z_p \quad \text{for} \quad z_p \geq S \tag{122}$$

$$\overline{\eta}_p = P_w z_b + (1 - P_w) S \quad \text{for} \quad z_p < S \tag{123}$$

The upper bound of $\overline{\eta}_p$ for $P_w = 1$ is the upper boundary of the permeable layer located at $z = z_b$. The lower bound of $\overline{\eta}_p$ for $P_w = 0$ is the higher elevation of the lower boundary z_p of the permeable layer and the still water level S. The wet probability P_w in Eq. (121) ensures that $q_p = 0$ if $P_w = 0$. Eqs. (121)– (123) based on physical reasoning may be crude but are used along with Eqs. (118) and (119) to estimate q_p for the known $\overline{h}$ and P_w.

The momentum flux in Eq. (116) is expressed as

$$\overline{u_b w}_p = \alpha_m P_w \left(g \overline{h} \right)^{0.5} w_m \tag{124}$$

with

$$\left(\alpha_p + \beta_1 w_m\right) w_m = g \tag{125}$$

where α_m =empirical parameter; and w_m = maximum downward seepage velocity due to the gravity force, obtained by solving Eq. (125) analytically. The seepage velocity w_p is assumed to be of the order of w_m or less. The horizontal velocity u_b at $z = z_b$ is assumed to be of the order of $\left(g\bar{h}\right)^{0.5}$. Eq. (124) assumes that the downward flux of the horizontal momentum during the wet duration is much larger than the upward momentum flux from the permeable layer.

The cross-shore variation of the mean water depth $\bar{h}$ is obtained by solving the momentum equation (116) together with the continuity equation (120). The probability density function $f(h)$ in the wet and dry zone is assumed to be exponential and given by

$$f(h) = \frac{P_w^2}{\bar{h}} \exp\left(-P_w \frac{h}{\bar{h}}\right) \quad \text{for} \quad h > 0 \tag{126}$$

with

$$P_w = \int_0^\infty f(h)dh \quad ; \quad \bar{h} = \int_0^\infty hf(h)dh \tag{127}$$

Eqs. (126) and (127) are the same as Eqs. (89) and (89) but presented again for clarity. The wet probability P_w equals the probability of the instantaneous water depth $h > 0$. The dry probability of $h = 0$ is equal to $(1 - P_w)$. The mean water depth for the wet duration is $\bar{h}$ but the mean depth for the entire duration is equal to $P_w\bar{h}$. The free surface elevation η above SWL is given by $\eta = \left(h + z_b - S\right)$ where z_b and S are assumed to be invariant during the averaging. The standard deviations of η and h are the same and given by

$$\frac{\sigma_\eta}{\bar{h}} = \left(\frac{2}{P_w} - 2 + P_w\right)^{0.5} \tag{128}$$

which is the same as Eq. (91).

The cross-shore velocity U may be related to the depth h in the wet and dry zone in the same way as in Eq. (92)

$$U = \alpha\sqrt{gh} + U_s \tag{129}$$

where α = positive constant taken as $\alpha = 2$; and U_s = steady velocity which is allowed to vary with x. The steady velocity U_s is included to account for offshore return flow on the seaward slope and crest and the downward velocity increase on the landward slope. Using Eqs. (126) and (129), the mean $\bar{U}$ and standard deviation σ_U of the cross-shore velocity U can be expressed as

$$\bar{U} = \frac{\sqrt{\pi}}{2}\alpha\left(P_w g\bar{h}\right)^{0.5} + P_w U_s \tag{130}$$

$$\sigma_U^2 = \alpha^2 g\bar{h} - 2\left(\bar{U} - U_s\right)\left(\bar{U} - P_w U_s\right) + P_w\left(\bar{U} - U_s\right)^2 \tag{131}$$

Eqs. (128), (130) and (131) express σ_η, $\bar{U}$ and σ_U in terms of $\bar{h}$, P_w and U_s which vary with x.

Eq. (129) is substituted into Eqs. (116) and (120) which are averaged for the wet duration using Eq. (126). The continuity equation (120) yields

$$\frac{3\sqrt{\pi}\alpha}{4}\bar{h}\left(\frac{g\bar{h}}{P_w}\right)^{0.5} + U_s\bar{h} = q \quad ; \quad q = q_o - q_p \tag{132}$$

where q = volume flux above the permeable layer. After lengthy algebra, the momentum equation (116) is expressed as

$$\frac{d}{dx}\left(B\frac{g\bar{h}^2}{P_w}+\frac{q^2}{\bar{h}}\right)=-g\bar{h}\frac{dz_b}{dx}-\frac{f_b}{2}\alpha^2 g\bar{h}G_b(r_s)-\alpha_m P_w\left(g\bar{h}\right)^{0.5}w_m \tag{133}$$

with

$$B=\left(2-\frac{9\pi}{16}\right)\alpha^2+1 \quad ; \quad r_s=\frac{3\sqrt{\pi}}{4}\frac{U_s\bar{h}}{q-U_s\bar{h}} \tag{134}$$

where the parameter B is related to the momentum flux term on the left hand side of Eq. (116).

The function $G_b(r_s)$ in Eq. (133) is given by Eqs. (98) and (99).

Eqs. (132) and (133) are used to predict the cross-shore variation of $\bar{h}$ and U_s for assumed q_o. It is necessary to estimate the wet probability P_w empirically. To simplify the integration of Eq. (133), the following formula is adopted:

$$P_w=\left[(1+A_1)\left(\frac{\bar{h}_1}{\bar{h}}\right)^n-A\left(\frac{\bar{h}_1}{\bar{h}}\right)^3\right]^{-1} \quad ; \quad A=\frac{q^2}{Bg\bar{h}_1^3} \quad ; \quad A_1=\frac{q_1^2}{Bg\bar{h}_1^3} \tag{135}$$

where $\bar{h}_1$ and $q_1=$ mean water depth and volume flux, respectively, at the location of $x = x_1$ where $P_w = 1$; $n =$ empirical parameter for P_w ; and A and $A_1 =$ dimensionless variables related to q and q_1, respectively. The transition from the wet ($P_w = 1$ always) zone to the wet and dry ($P_w < 1$) zone may be taken at $x_1 = x_{SWL}$ where x_{SWL} is the cross-shore location of the still water shoreline of an emerged crest as shown in Fig. 6. Eq. (135) is assumed to be valid on the upward slope and horizontal crest in the region of $x_1 \le x \le x_c$ where x_c is the highest and most landward location of the structure.

Integration of Eq. (133) for P_w given by Eq. (135) starting from $\bar{h}=\bar{h}_1$ at $x=x_1$ yields $\bar{h}(x)$

67

$$B_n\left(1+A_1\right)\bar{h}_1\left[\left(\frac{\bar{h}_1}{\bar{h}}\right)^{n-1}-1\right]=z_b(x)-z_b(x_1)+\int_{x_1}^{x}\left[\frac{f_b}{2}\alpha^2 G_b+\alpha_m\frac{P_w w_m}{\left(g\bar{h}\right)^{0.5}}\right]dx \qquad (136)$$

where $B_n = B(2-n)/(n-1)$; and $z_b(x)$ = bottom elevation at the cross-shore location x. The mean water depth $\bar{h}$ at given x is computed by solving Eq. (136) iteratively. The empirical parameter n is taken to be in the range of $1 < n < 2$ so that $B_n > 0$. The formula for n for the impermeable wet and dry zone in Section 8.1 is adopted and expressed as $n = 1.01 + 0.98\left[\tanh\left(A_o\right)\right]^{0.3}$ where $1.01 \le n \le 1.99$ and $A_o = q_o^2/\left(Bg\bar{h}_1^{3}\right)$.

On the downward slope in the region of $x > x_c$, the wet probability P_w is assumed to be given by

$$P_w^{-1}=P_c^{-1}+\frac{q_c^2-q^2}{Bg\bar{h}^3} \qquad (137)$$

where P_c and q_c are the computed wet probability P_w and volume flux q at $x = x_c$. Substituting Eq. (137) into Eq. (133) and integrating the resulting equation from x_c to x, the mean depth $\bar{h}(x)$ is expressed as

$$\frac{\bar{h}}{\bar{h}_c}-1+\frac{P_c q_c^2}{4gB\bar{h}_c^3}\left[\left(\frac{\bar{h}_c}{\bar{h}}\right)^2-1\right]=\frac{P_c}{2B\bar{h}_c}\left\{z_b(x_c)-z_b(x)-\int_{x_c}^{x}\left[\frac{f_b}{2}\alpha^2 G_b+\alpha_m\frac{P_w w_m}{\left(g\bar{h}\right)^{0.5}}\right]dx\right\} \qquad (138)$$

where $\bar{h}_c$ is the computed mean depth at $x = x_c$.

The wave overtopping rate q_o is predicted by imposing $U_s = 0$ in Eq. (132) at the crest location x_c

$$q_o = \frac{3\sqrt{\pi}\alpha}{4}\bar{h}_c\left(\frac{g\bar{h}_c}{P_c}\right)^{0.5} + q_p \qquad \text{at } x = x_c \qquad (139)$$

The wave overtopping probability P_o may be related to the wet probability P_c at $x = x_c$ where both P_o and P_c are in the range of 0.0 – 1.0. The empirical relation of $P_o = \left[\tanh\left(5P_c\right)\right]^{0.8}$ for the impermeable wet and dry zone in Section 8.1 is adopted to estimate P_o.

For assumed q_o, the landward marching computation of $\bar{h}, \sigma_\eta, \bar{U}$ and σ_U is initiated using the wet model in Section 6 from the seaward boundary $x = 0$ to the landward limit located at $x = x_r$. The landward marching computation is continued using the wet and dry model in this section from the location of $x = x_{\mathrm{SWL}}$ where $\bar{h} = \bar{h}_1$ to the landward end of the computation domain or until the mean depth $\bar{h}$ becomes less than 0.001 cm. The rate q_o is computed using Eq. (139) together with the overtopping probability P_o. This landward computation starting from $q_o = 0$ is repeated until the difference between the computed and assumed values of q_o is less than 1%. This convergency is normally obtained after several iterations. The computed values of $\bar{h}, \sigma_\eta, \bar{U}$ and σ_U by the two different models in the overlapping zone of $x_{\mathrm{SWL}} < x < x_r$ (see Fig. 6) are averaged to smooth the transition from the wet zone to the wet and dry zone.

Farhadzadeh et al. (2009) compared the numerical model with S, OS and O test series explained by Kobayashi and de los Santos (2007) and D' test series by van Gent (2002). The number of tests varied from 10 to 18 for the four test series. The total number of tests was 52. The seaward slope was in the range of 1/5 to 1/2. The nominal stone diameter D_{n50} varied from 0.49 to 4.23

cm. The maximum vertical thickness t_a of the armor layer was in the range of 0.49 to 14.0 cm where t_a corresponds to the maximum value of $[z_b(x) - z_p(x)]$ in Fig. 6. The measured porosity of the stone was $n_p = 0.5$ for S and OS test series. The same value of n_p is used for O and D' test series. The maximum downward seepage velocity w_m estimated using Eq. (125) along with Eq. (119) and $\nu = 0.01$ cm^2/s is in the range of 4.4 to 14.3 cm/s. The still water level S, root-mean-square wave height H_{rms}, and spectral peak period T_p measured at the offshore boundary $x = 0$ for each test are specified as input to the numerical model.

Initially, the downward momentum flux was neglected in Eq. (116), corresponding to $\alpha_m = 0$ in the present numerical model. The computed wave overtopping rates for $\alpha_m = 0$ were too large by one order of magnitude probably because the permeable layer above SWL may not be saturated and accept larger fluxes of water volume and momentum. The empirical formula developed using the 52 tests was expressed as

$$\alpha_m = \alpha \left(\frac{z_b - z_p}{D_{n50}} \right)^{0.3}$$

(140)

where the constant α is the same as $\alpha = 2$ in Eq. (129) and $(z_b - z_p)/D_{n50}$ is the local thickness of the permeable layer normalized by the nominal stone diameter. This thickness correction reduces the computed q_o for S and OS test series with $t_a / D_{n50} = 4.1$. For O and D' test series, $\sigma_m \simeq \alpha$ on the permeable layer. Eq. (140) ensures $\alpha_m = 0$ in the zone of $z_b = z_p$ and no permeable layer. The measured and computed wave overtopping rates q_o were compared for O, S, OS and D' test series. The wave overtopping probability P_o was measured for O and D' test series. The agreement for q_o and P_o was mostly within the factor of about 2.

70

For D' test series, van Gent (2002b) measured the water depth and velocity at five points for each test. Points P1 and P2 were located at the seaward and landward ends of the crest, respectively. Points P3, P4 and P5 were located on the landward slope at elevations of 10, 25 and 40 cm, respectively, below the crest. The measured water depth and velocity at each point were analyzed on the basis of individual wave overtopping events. The values tabulated in his report were the water depth $h_{2\%}$, velocity $U_{2\%}$, and discharge $q_{2\%}$ corresponding to the values exceeded by 2% of the incident 1,000 waves.

For the probability density function $f(h)$ given by Eq. (126), the water depth h_e corresponding to the exceedance probability e is given by

$$h_e = \frac{\overline{h}}{P_w} \ln\left(\frac{P_w}{e}\right) \quad \text{for} \quad P_w > e \tag{141}$$

Using Eq. (129), the water velocity U_e and discharge q_e corresponding to the exceedance probability e are expressed as

$$U_e = \alpha\sqrt{gh_e} + U_s \quad ; \quad q_e = h_e U_e \tag{142}$$

The probability e of $h > h_e$ at given x is not directly related to the probability based on individual overtopping events. The probability 2% used by van Gent (2002b) is assumed to correspond to the range of $e = 0.01 - 0.02$ where Eq. (141) is not very sensitive to $e = 0.01 - 0.02$ as long as the wet probability P_w is larger than about 0.1. The computed values of h_e, U_e and q_e in CSHORE2009 are based on $e = 0.01$ where use is made of $e = P_w/1.1$ if $P_w < 0.011$ so that $(P_w/e) \geq 1.1$ in Eq. (141). Farhadzadeh et al. (2009) compared the measured and computed values of $h_{2\%}$, $U_{2\%}$ and $q_{2\%}$, respectively, at the five points P1 to P5 for D' test series.

The agreement was mostly within the factor of 2 but the hydrodynamic variables in the wet and dry zone are difficult to predict accurately due to the small water depth and larger velocity during intermittent wave overtopping.

9.2 Stone Movement

The sediment transport model for the impermeable sand beach in Sections 5 and 8.2 is modified to predict the movement of stone armor units on a coastal structure. The probability P_b of stone movement under the Gaussian velocity U in the wet zone is estimated assuming that the stone movement occurs when the absolute value of the instantaneous velocity U exceeds the critical velocity U_{cb} estimated as

$$U_{cb} = \left[N_c g (s-1) D_{n50} \right]^{0.5} \tag{143}$$

where s and D_{n50} = specific gravity and nominal diameter of the stone; and N_c = empirical parameter. If the wave height H_c corresponding to U_{bc} is given by $H_c = U_{bc}^2 / g$, Eq. (143) yields $N_c = H_c / \left[(s-1) D_{n50} \right]$ and N_c may be regarded as the critical stability number for the stone which is of the order of unity (Kobayashi et al. 2003). Eq. (49) is based on the critical Shields parameter $\Psi_c = 0.05$ for the initiation of sand movement. The two parameters are related by $N_c = 2\Psi_c / f_b$ and Eq. (49) for the probability P_b is applicable using $\Psi_c = 0.5 f_b N_c$. Eq. (143) is adopted here and N_c is calibrated as $N_c = 0.7$ using the damage progression tests of a stone structure with $s = 2.66$ and $D_{n50} = 3.64$ cm conducted by Melby and Kobayashi (1998). The probability of stone suspension is estimated using Eq. (50) where the stone fall velocity w_f is estimated using $w_f = 1.8 \left[g (s-1) D_{n50} \right]^{0.5}$ for a sphere (e.g., Jiménez and Madsen 2003). For

the stone with $s = 2.66$ and $D_{n50} = 3.64$ cm, $w_f = 1.4$ m/s and the computed probability of suspension of this stone is essentially zero. The stone armor units are assumed to move like bedload particles, although CSHORE2009 also computes the suspended stone transport rate using the formulas developed for sand.

The probability P_b of stone movement in the wet and dry zone is obtained for the probability distribution of U based on Eqs. (126) and (129). The probability P_b of stone movement is assumed to be the same as the probability of $|U| > U_{cb}$ with U_{cb} given by Eq. (143). Then, P_b is given by Eqs. (105) – (107).

The time-averaged volumetric rate q_b of stone transport is estimated using the formula for bedload given by Eq. (114) which is modified as

$$q_{bx} = b P_b G_s B_r \sigma_U^3 / \left[g(s-1) \right] \quad ; \quad B_r = \left(\frac{z_b - z_p}{D_{n50}} \right)^m \leq 1 \tag{144}$$

where b = bedload parameter specified as $b = 0.002$ as discussed below Eq. (57); G_s = function of the bottom slope given by Eqs. (58) and (59); B_r = reduction factor due to limited stone availability; m = empirical parameter; and σ_U = velocity standard deviation representing the wave action on the stone. The rate q_{bx} becomes negative (offshore) on the steep slope with $G_s < 0$. The reduction factor B_r is added in CSHORE2009 to account for the thickness $(z_b - z_p)$ of the stone layer where $B_r = 1$ if $(z_b - z_p) > D_{n50}$ and $B_r = 0$ in the zone of $z_b = z_p$ and no stone. The computed profile changes are found to be insensitive to the parameter m in the

73

range of 0.5 to 2.0. The value of $m = 1.0$ is specified in CSHORE2009. The rate q_{bx} of stone transport in the wet and dry zone is also estimated using Eq. (144) where the parameter b is chosen so that the values of q_{bx} computed for the two different zones are the same at the still water shoreline located at $x = x_{SWL}$. The computed cross-shore variations of q_{bx} in the two zones are averaged in the overlapping zone of $x_{SWL} \leq x \leq x_r$ for the smooth transition between the two zones. The temporal change of the bottom elevation z_b is computed using the conservation equation of stone volume in the same way as in Section 8.2.

Farhadzadeh et al. (2009) compared the numerical model with the three damage progression tests by Melby and Kobayashi (1998). The armor stone was placed in a traditional two-layer thickness with the seaward slope of 1/2. The armor stone was characterized by $D_{n50} = 3.64$ cm, $s = 2.66$ and $n_p = 0.4$ where the maximum seepage velocity was $w_m = 8.7$ cm/s using Eq. (125). The thickness of the armor layer was 7.3 cm. The test duration was in the range of 8.5 to 28.5 h. The numerical model overpredicted the deposited area below SWL at the end of the test mostly because it does not account for discrete stone units dislodged and deposited at a distance seaward of the toe of the damaged armor layer. The eroded area above SWL was predicted better. The temporal variation of the eroded area A_e was compared using damage S_e defined as $S_e = A_e / D_{n50}^2$. The numerical model predicted the damage progression well partly because the critical stability number N_c introduced in Eq. (143) was calibrated to be $N_c = 0.7$ for the three damage progression tests. The temporal variations of S_e computed for $N_c = 0.7$ and 0.6 were fairly sensitive to N_c. The simple criterion of stone movement based on Eq. (143) may be improved so as to predict the damage progression more accurately.

10. Computer Program CSHORE2009

The computer program CSHORE2009 is explained sufficiently so that users will be able to use it effectively and modify it if necessary. CSHORE2009 provides various options but only certain combinations of the options have been applied and verified in the publications in Section 2. Enough explanations are provided in the computer program so that users will be able to follow the computer program with additional explanations provided in the following. It is noted that the symbols used in this section are based on those used in the computer program rather than those used in the previous sections.

10.1 Main program

The wave action equations (36) and (63), the momentum equations (22) and (23), and the roller energy equation (41) and the equations (101), (104), (136) and (138) for the mean water depth $\overline{h}$ in the wet and dry zone are solved using the finite-difference method with constant nodal spacing Δx of a sufficient resolution in very small water depth. The use of constant small Δx may be justified because CSHORE is very efficient computationally and the use of constant Δx reduces the input preparation time. It is noted that the governing equations (22), (23), (36), (41) and (63) divided by ρg are solved in the main program so that the fluid density ρ does not appear in the resulting equations.

The differential equations solved numerically can be expressed in the form

$$\frac{dy}{dx} = f(x, y)$$

where x = cross-shore coordinate, positive onshore; y = unknown variable that needs to be computed; and f = known function of x and y. The computation marches landward from the given x to the next nodal location at $(x + \Delta x)$. An improved Euler method of second-order accuracy (e.g., Chaudhry 1993) is used to approximate the above equation as follows:

$$\text{Predictor: } y_{j+1}^* = y_j + f(x_j, y_j) \Delta x$$

$$\text{Corrector: } y_{j+1} = y_j + \frac{1}{2} \left[f(x_j, y_j) + f(x_{j+1}, y_{j+1}^*) \right] \Delta x$$

where the subscripts j and $(j+1)$ indicate the nodes located at x_j and $x_{j+1} = (x_j + \Delta x)$ and the superscript star denotes a temporary value of y_{j+1} at node $(j+1)$. The wave action equation (36) or (63) for the free surface standard deviation σ_η, the cross-shore momentum equation (22) for the wave setup $\overline{\eta}$, and the roller equation (41) for the roller volume flux q_r are solved using this Euler method. On the other hand, the longshore momentum equation (23) is approximated by an implicit finite-difference method, which is more stable numerically, to obtain the longshore bottom shear stress τ_{by} at node $(j+1)$ and the corresponding longshore current $\overline{V}$ at node $(j+1)$.

In reality, the four unknown values of $\sigma_\eta, \overline{\eta}, \overline{V}$ and q_r at node $(j+1)$ involved in the four differential equations are computed in sequence and iteratively. The mean water depth $\overline{h}$ given by Eq. (1) is uniquely related to the wave setup $\overline{\eta}$ for the given storm tide S and bottom elevation z_b. The convergence of the iteration is based on the difference between the computed

and guessed values where the metric units are used in the computer program and the gravitational acceleration g = 9.81 m/s². The difference for σ_η (m), $\bar{h}$ (m), and $\bar{V}$ (m/s) must be less than EPS1, whereas the difference for q_r (m²/s) must be less than EPS2. The maximum number of the iteration is MAXITE. The DATA statement in the main program specifies EPS1=10⁻³, EPS2=10⁻⁶ and MAXITE=20 where double precision is used in the entire program. It is noted that q_r involves the product of the length and velocity.

The only input in the main program is as follows:

```
            WRITE(*,*) 'Name of Primary Input-Data-File?'
C           READ(*,5000) FINMIN
            FINMIN = 'infile'
      5000  FORMAT(A12)
```

where FINMIN corresponds to the name of the input file which will be read later before the computation. In order to eliminate this input, the name of the input file is specified as *infile* in CSHORE.

10.2 Subroutines

Subroutines are arranged in numerical order after the main program in order to indicate the location of each subroutine in the computer program. The numerical order approximately corresponds to the chronology of the CSHORE development summarized in Section 2.

Subroutine 1 **OPENER** opens all input and output files. The input file with its name = FINMIN is assigned to unit=11 for the READ statement. The names of the output files start with the letter

O. The output file ODOC (unit=20 for the WRITE statement) is used to store the input (to check the accuracy of the input file) and the summary of the computed results (to check the overall appropriateness of the computed results and to compare with measurements such as wave runup and overtopping rates). The output file OMESSG (unit=40) stores warning and error messages generated during the computation. These messages must be examined carefully if the computed results appear questionable. The other output files are explained in Section 10.4.

Subroutine 2 **INPUT** reads the contents of the input file FINMIN as explained in detail in section 10.3. The gravitational acceleration g is specified as GRAV=9.81 m/s^2 in the DATA statement.

Subroutine 3 **BOTTOM** calculated the bottom elevation $z_b(x_j)$ with $x_j = (j-1)\Delta x$ at node j using the input bottom elevations specified at a number of cross-shore locations. The nodal spacing Δx is read from the input file. Use is made of linear interpolation and smoothing to reduce sharp corners that tend to cause numerical irregularity. This subroutine also computes the integer JMAX which is the number of total nodes along the bottom in the computation domain as well as the cross-shore bottom slope S_{bx} of the smoothed z_b. If the bottom is permeable or the sediment layer thickness is thin, the lower impermeable boundary elevation z_p of the permeable or thin sediment layer (see Figs. 2 and 6) is calculated in the same way as z_b. The thickness h_p of the layer is obtained using $h_p = (z_b - z_p) \geq 0$. For the permeable layer, h_p is the thickness of porous flow. For the thin sediment layer, h_p is the available deposited sediment volume per unit horizontal area.

Subroutine 4 **PARAM** computes constant parameters before the landward marching computation. Eqs. (65) and (66) are used to compute the values of α_p, β_1 and β_2 using the default values of $\nu = 10^{-6}$ m^2/s, $\alpha_0 = 1000$ and $\beta_0 = 5$. The default value of $\alpha = 2$ in Eq. (92) for the wet and dry zone is specified and the value of B defined in Eq. (97) and other constant parameters are calculated. The exceedance probability $e = $ EWD introduced in Eq. (141) specified as 0.015 for an impermeable bottom and 0.01 for a permeable bottom on the basis of the comparison with the data by Van Gent (2002b).

Subroutine 5 **LWAVE** solves the dispersion relation for linear waves given by Eq. (2) which is rewritten in terms of $x = k\overline{h}$

$$x - D\left(1 - \frac{T_p Q}{2\pi \overline{h}^2} x\right)^2 \coth(x) = 0$$

with

$$D = k_o \overline{h} \quad ; \quad Q = Q_x \cos\theta + Q_y \sin\theta$$

where T_p = representative wave period at $x = 0$ specified as input; $\overline{h}$ = mean water depth at given node; k_o = deep water wave number given by $k_o = (2\pi)^2 / (gT_p^2)$ calculated in subroutine 4 PARAM or at the end of the main program if additional wave conditions are specified as input at the seaward boundary $x = 0$. The above equation is solved using the Newton-Raphson method (e.g., Press et al. 1989). After the wave number $k = x/\overline{h}$ is obtained, the linear wave quantities such as those defined in Eq. (3) are computed and the wave angle θ for obliquely incident waves is calculated using Eq. (21). CSHORE provides the option of IWCINT=0 or 1. IWCINT=0 corresponds to the case of no wave and current interaction, which was assumed in

the earlier version of CSHORE developed for the condition of no or little wave overtopping. IWCINT=1 corresponds to the present version of CSHORE which allows considerable wave overtopping and overflow. If IWCINT=0, the terms involving Q_x and Q_y in Eqs. (2), (22), (23) and (36), and (63) are neglected and $Q = 0$ in the above equation for $x = k\overline{h}$.

Subroutine 6 **GBXAGF** computes G_{bx} and G_f using the approximate equations (46) and (48) for obliquely incident waves and the exact equations given by Kobayashi et al. (2007b) for normally incident waves. The complementary error function *erfc* involved in the exact equations is computed using Function **ERFCC** given by Press et al. (1989). Subroutine 6 **VSTGBY** computes $V_* = \overline{V} / \sigma_T$ for known G_{by} using Eq. (47). The longshore momentum equation (23) is solved numerically to obtain τ_{by} and the corresponding G_{by} is calculated using Eq. (33).

Subroutine 7 **DBREAK** computes the energy dissipation rate D_B due to wave breaking using Eq. (38) and specifies the upper limit of unity for $\sigma_* = \sigma_\eta / \overline{h}$ in the wet zone of very shallow water. The other limit of σ_* introduced for irregular wave transmission over submerged porous breakwaters by Kobayashi et al. (2007b) has been found to be unnecessary for the other applications of CSHORE discussed in Section 2. An option is provided for estimating the breaker ratio parameter γ in Eq.(38) using the empirical formula proposed by Apotsos et al. (2008). This option is adopted if the input value of γ is negative.

Subroutine 8 **OUTPUT** stores most of the computed results in the output files as explained in detail in Section 10.4.

Subroutine 9 **POFLOW** computes the standard deviation σ_p of the discharged velocity in a permeable layer using Eq. (72), the mean cross-shore discharge velocity $\overline{U}_p$ using Eq. (70), and the energy dissipation rate D_p due to flow resistance in the permeable layer using Eq. (68). CSHORE provides the option of IPERM = 0 or 1. IPERM=0 implies an impermeable bottom and this subroutine is not called from the main program. IPERM=1 implies that a permeable layer exists in the computation domain where the permeable layer thickness $h_p = 0$ for impermeable segments.

Subroutine 10 **QORATE** is called from the main program after the landward marching computation in the wet zone if the option of IOVER=1 is specified as input to allow wave overtopping and overwash in the computation domain. No wave overtopping is allowed if IOVER=0 and the wave overtopping rate $q_o = 0$ in Eqs. (19) and (62). The wave overtopping rate q_o is obtained by calling subroutine 16 WETDRY. After the convergence of repeated landward computations to obtain q_o, the quantities related to wave runup are computed using the equations in Section 7. Eqs. (141) and (142) are used to compute h_e, U_e and q_e corresponding to the specified exceedance probability e.

Subroutine 11 **SEDTRA** computes the sediment transport quantities in the wet zone using the equations in Section 5 after the landward marching computation of the hydrodynamic quantities

81

is completed. This subroutine is called from the main program only for the option of IPROFL=1, corresponding to a movable bottom. For a fixed bottom, IPROFL=0 must be specified as input. The computation is performed separately for normally incident waves (integer IANGLE=0) and for obliquely incident waves (IANGLE=1) partly because of the CSHORE development history discussed in Section 2 and partly because of no longshore sediment transport for IANGLE=0. The sediment transport quantities in the wet and dry zone are computed using the equations in Sections 8.2 and 9.2 only for IANGLE=0 and IOVER=1.

Subroutine 12 **CHANGE** computes the bottom elevation change from the present time level to the next time level using Eq. (61) with $\partial q_y / \partial y = 0$. The finite difference equations for the profile change computation given by Tega and Kobayashi (1999) are of second-order accuracy. The time step Δt for the profile change computation is computed using the numerical stability criterion of the adopted explicit finite difference method. The profile change is computed if IPROFL=1.

Subroutine 13 **INTGRL** integrates a function numerically using a modified Simpson's rule (e.g., Press et al. 1989). This subroutine is used in Subroutine CHANGE to ensure that the computed profile change satisfies the conservation of the sediment volume in the entire computation domain.

Subroutine 14 **SMOOTH** smoothes the cross-shore variation of a variable that depends on x. Simple moving averaging is performed using NPT nodes landward and seaward of a specified node. NPT=0 corresponds to no smoothing. The smoothing of certain variables reduces sudden

changes and improves numerical stability. Some variables are smoothed before their storage and plotting. The value of NPT is calculated in Subroutine 03 BOTTOM before the computation and at the end of Main Program during the computation. The calculated value of NPT increases with the ratio between the input wave height and the nodal spacing Δx so that the smoothing distance is more related to the input root-mean-square wave height.

Subroutine 15 **EXTRAPO** called from Subroutine SEDTRA is used to extrapolate a finite sediment transport rate at the landward end node of the computation to zero transport rate on the landward dry zone after the introduction of the scarping algorithm given by Eq. (60). The number of nodes for the extrapolation is specified by NPE. The value of NPE is calculated in a manner similar to the calculation of NPT. If wave overwash is allowed by choosing the option IOVER=1, this subroutine is not used.

Subroutine 16 **WETDRY** computes the hydrodynamic quantities including the wave overtopping rate q_o in the wet and dry zone using the equations in Sections 8.1 and 9.1. Function GBWD following this subroutine computes the value of $G_b(r)$ for given r using Eqs. (98) and (99).

Subroutine 17 **TRANWD** called from the main program and subroutine SEDTRA connects the computed values by the wet model and the wet and dry model in the overlapping zone (see Figs. 5 and 6) because the transition between the two different models is somewhat artificial. The overlapping zone and transition algorithm are discussed at the end of Sections 8.1 and 9.1.

Subroutine 18 **PROBWD** computes the probabilities of sediment movement and suspension using Eqs. (105), (106) and (107) as well as Eqs. (108), (109) and (110) where only the critical fluid velocities U_{cb} and U_{cs} are different in these equations.

Subroutine 19 **TSMOTH** converts time series stored at arbitrary time levels in Main Program to smoothed time series with a constant time interval. This subroutine is created to store the computed wave overtopping rate q_o and the computed bedload transport rate q_{bx} and suspended sediment transport rate q_{sx} at the landward end node JMAX if IPROFL=1 and IOVER=1. The time step Δt for the profile change computation using Eq. (61) is not constant and the time series are stored at the time level of the profile change computation. The stored values of q_o, q_{bx} and q_{sx} in the zone of the very small water depth can be noisy and smoothed.

Subroutine 20 **TSINTP** interpolates time series specified at given time levels, obtains interpolated time series at different time levels, and converts interpolated time series into time series with stepped temporal changes. This subroutine is created in relation to the option of ILAB=0 or 1 in Subroutine 02 INPUT. For ILAB=0 corresponding to typical field data, the time series of the input wave parameters and water levels have different time intervals and are read separately as explained in Section 10.3.

10.3 Input

A user of CSHORE must read Subroutine 2 **INPUT** and learn how to prepare the primary input data file. Input parameters and variables are read using the FORMAT statements at the end of Subroutine INPUT. A user must follow the FORMAT requirements so that a correct input value

is assigned to the specific input parameter or variable. This requirement may not be convenient but the resulting input file is orderly and can be checked easily. In the following, the input parameters and variables are explained in the sequence described in Subroutine INPUT.

- NLINES is the number of lines used to identify a specific input file because a number of input files can become large when CSHORE is compared with a number of data sets with different bottom profiles.

- (COMMEN(J), J=1, 14) read for NLINES lines contains the description of the input file. The comments in these lines do not affect the computed results at all.

- IPROFL = 0 or 1 for a fixed or movable bottom where the profile evolution is computed for IPROFL=1.

- ISEDAV=0 or 1 for unlimited or limited sediment availability. ISEDAV=0 is already specified if IPROFL=0. If IPROFL=1, ISEDAV=0 or 1 must be specified. The option of ISEDAV=1 has been used only for stone movement in Section 9.2 so far.

- IPERM = 0 or 1 for an impermeable or permeable bottom where the parameters for the permeable layer must be specified later if IPERM=1.

- IOVER = 0 or 1 for no wave overtopping or wave overtopping at the landward end of the computation domain where wave overwash and dune profile evolution are computed if IOVER=1 and IPROFL=1.

- IWTRAN=0 or 1 for no standing water or wave transmission in a bay or lagoon landward of an emerged dune or coastal structure. IWTRAN=0 is already specified if IOVER=0. If IOVER=1, IWTRAN=0 or 1 must be specified. The option of IWTRAN=1 has not been used so far.

- IWCINT = 0 or 1 for no or yes for wave and current interactions where the terms involving Q_x and Q_y in Eqs. (2), (22), (23), (36) and (63) for the wet zone are neglected if IWCINT=0. Wave and current interactions are not negligible if the current velocity becomes as large as the wave phase velocity C. The effect of wave overtopping on the hydrodynamics in the wet and dry zone is included in the models in Sections 8.1 and 9.1.

- IROLL = 0 or 1 for no or yes for roller effects in the wet zone where the roller volume flux $q_r = 0$ and $D_r = D_B$ in Eq. (41) for IROLL=0. The option IROLL=1 improves the prediction of longshore current on a beach and dune erosion but the roller effects have found to be negligible for coastal structures with steeper slopes, perhaps because of the limited horizontal distance for roller development. The roller effect in the wet and dry zone may have been included implicitly because of the use of Eq. (92).

- IWIND = 0 or 1 for no or yes for wind effects where the wind stresses τ_{sx} and τ_{sy} on the sea surface are neglected in Eqs. (22) and (23) if IWIND=0. The wind effect is normally small unless the computation domain becomes large.

- DX = constant nodal spacing $\Delta x(m)$. The value of $x_s / \Delta x$ with x_s = cross-shore distance between the seaward boundary $x = 0$ and the shoreline located at the bottom elevation $z_b = 0$ was of the order of 1,000 for the previous computations. The values of Δx were of the order of 0.01 m and 1.0 m for laboratory and field data, respectively. The integer NN in the PARAMETER statement specifies the maximum number of nodes allowed in the computation domain. The default value of NN = 200,000 should be sufficient for any CSHORE computation.

- GAMMA = empirical breaker ratio parameter γ in Eq. (38) where the range of $\gamma = 0.5 - 1.0$ has been used to adjust the computed cross-shore variation of the wave height in comparison with the measured wave height variation. If no wave height data is available, use may be made of $\gamma = 0.7$ or 0.8. Alternatively, the empirical formula proposed by Apotsos et al. (2008) may be used for natural beaches but this formula has not been verified yet for the prediction of morphological changes.

- D50, WF and SG = median sediment diameter d_{50} (mm) which is immediately converted to $d_{50}(m)$, sediment fall velocity w_f (m/s), and sediment specific gravity s if IPROFL=1. The default values for the sediment in subroutine INPUT are the sediment porosity SPORO = n_p = 0.4 in Eq. (61), the critical Shields parameter ψ_c = 0.05 for Eq. (49), the critical stability number N_c = 0.7 in Eq. (143), the critical sediment diameter CSEDIA=0.01 (m) used for the movement initiation of sand (ψ_c = 0.05 if D50 < CSEDIA) and stone (N_c = 0.7 if D50 $\geq$

CSEDIA) and the parameter BEDLM = m = 1.0 in Eq. (144) for bedload reduction due to limited availability.

- EFFB, EFFF, SLP, SLPOT = suspension efficiency e_B due to wave breaking in Eq. (51), suspension efficiency e_f due to bottom friction in Eq. (51), suspended load parameter a in Eq. (52), and suspended load parameter a_o associated with the wave overtopping rate q_o in Eq. (113). These input parameters are required only if IPROFL=1. The input of SLPOT = a_o is required only if IOVER=1. The calibrated ranges of these parameters are $e_B = 0.002 - 0.01$ (typically 0.005), $e_f = 0.01$ (fixed in the previous calibrations), $a = 0.1 - 0.4$ (typically 0.2), and $a_o = 0.1 - 2.8$ (typically 0.5 but calibrated only for limited wave overwash data). It is required that $e_B < e_f$ because the turbulence generated by wave breaking decays downward before it suspends bottom sediment.

- TANPHI, BLP = sediment limiting (maximum) slope $\tan \phi$ in Eqs. (52), (58) and (59), and bedload parameter b in Eqs. (56) and (57) if IPROFL=1. These parameters related to bedload have been calibrated in the range of $\tan \phi = 0.63$ (fixed in the previous calibrations) and $b = 0.001 - 0.004$ (typically 0.002).

- RWH = runup wire height $\delta_r(m)$ shown in Fig. 3 only if IOVER=1. If no runup wire is deployed to measure irregular wave runup, use may be made of $\delta_r = 0.02$ m for small-scale experiments and $\delta_r = 0.1$ m for prototype beaches and structures. The range of $\delta_r = 0.01 -$ 0.1 m is realistic for a runup wire placed above a slope.

- SNP and SDP = porosity n_p and nominal diameter $D_{n50}(m)$ of stone used in Eqs. (65), (66) and (119) only if IPERM=1 and a permeable layer is constructed of stone. The maximum seepage velocity WPM = w_m is computed using Eq. (125). If other materials are used for slope protection, formulas corresponding to Eqs. (65), (66) and (119) will need to be developed. If IPROFL=1 and IPERM=1, SNP=SPORO and SDP=D50 where SDP(m) and D50 (mm) are read as input.

- ILAB=0 or 1 for reading the input wave and water level data separately or together where ILAB=1 for laboratory experiments in which offshore waves and water level are normally measured simultaneously.

- NWAVE = number of waves at the seaward boundary $x = 0$. If IPROFL=0 and the bottom is fixed, NWAVE is the number of different waves at $x = 0$ examined for this specific fixed bottom. If IPROFL=1 and the bottom profile evolves from the specified initial profile, NWAVE is the number of sequential waves at $x = 0$ during the profile evolution starting from the morphological time $t = 0$. It is noted that NWAVE must not exceed the integer NB in the PARAMETER Statement where NB=30,000 is specified.

- NSURG = number of water levels at the seaward boundary $x = 0$. NSURG must be equal to NWAVE if ILAB=1.

- TIMEBC(I+1), TPBC(I), HRMSBC(I), WSETBC(I), SWLBC(I), WANGBC(I) for I=1,2,…, NTIME only if ILAB=1 where NTIME = NWAVE = NSURG

    TIMEBC(I+1) = morphological time in seconds at the end of the I-th wave and water level during the profile evolution starting from TIMEBC(1) = 0.0. The wave conditions and water level during TIMEBC(I) to TIMEBC(I+1) are assumed to be constant and NTIME is the number of constant wave conditions and water level. For IPROFL=0, TIMEBC(I+1) = 1.0, 2.0, …, NTIME may be used to identify the sequence of the waves and water levels at $x = 0$ used for the computation.

    TPBC(I) = spectral peak period T_p (s) used to represent the I-th irregular wave period at $x = 0$ but any representative wave period can be specified.

    HRMSBC(I) = root-mean-square wave height $H_{rms} = \sqrt{8}\,\sigma_\eta$ (m) used to represent the I-th irregular wave height at $x = 0$. If the spectral significant wave height H_{mo} is known, the corresponding H_{rms} may be obtained using $H_{rms} = H_{mo} / \sqrt{2}$.

    WSETBC(I) = wave setup (positive) or set-down (negative) $\overline{\eta}$ (m) at $x = 0$ relative to the still water level (SWL). If $\overline{\eta}$ is not measured, use may be made of $\overline{\eta} = 0.0$ at $x = 0$ as long as the seaward boundary $x = 0$ is located outside the surf zone.

    SWLBC(I) = still water level S (m) above the datum $z = 0$ as shown in Fig. 2. This value of S corresponds to storm tide (sum of storm surge and tide) during the I-th wave conditions.

90

WANGBC(I) = incident wave angle θ in degrees at $x = 0$ for the I-th wave conditions (see

Fig. 1 for the definition of θ). The angle is limited to the range of $\theta = -80°$ to $80°$

because the formula for D_B given by Eq. (38) was originally developed for normally

incident waves and may not be valid for large incident wave angles. IANGLE=0 or 1 is

used to indicate normally or obliquely incident waves in the computer program.

If ILAB=0, NWAVE and NSURG are different and NTIME is taken as the larger value of

NWAVE and NSURG. For ILAB=0 corresponding to field data, offshore wave conditions and

water level at $x = 0$ are assumed to change continuously unlike laboratory wave conditions and

water level that are normally varied in steps. After the offshore wave data and the water level

data are read separately, Subroutine 20 TSINTP is called to create the stepped time series

corresponding to ILAB=1.

- TWAVE(I), TPIN(I), HRMSIN(I), WANGIN(I) for I=1, 2, …, (NWAVE+1) only for

  ILAB=0 where

    TWAVE(I) = time (s) of the I-th wave data where TWAVE(1)=0.0.

    TPIN(I) = spectral peak period T_p (s) at time = TWAVE(I).

    HRMSIN(I) = root-mean-square wave height H_{rms} (m) at time = TWAVE(I).

    WANGIN(I) = incident wave angle θ in degrees at time = TWAVE(I).

  The wave setup or set-down $\bar{\eta}$ at $x = 0$ is assumed to be zero for field data.

- TSURG(I), SWLIN(I) for I=1,2,…, (NSURG+1) only for ILAB=0 where

    TSURGE(I) = time (s) for the I-th water level where TSURG(1) = 0.0.

    SWLIN(I) = water level S (m) above $z = 0$ at time = TSURG(I).

  It is required that TWAVE (NWAVE+1) = TSURG (NSURG+1) because the durations of the wave data and water level data must be the same.

- NBINP = number of points used to describe the input bottom geometry $z_b(x)$ which is the initial profile if IPROFL=1. The bottom geometry is divided into linear segments of different inclination and roughness starting from the seaward boundary $x = 0$. It is noted that NBINP must not exceed NB = 30,000 in the PARAMETER statement.

- NPINP = number of points used to describe the input impermeable fixed boundary $z_p(x)$ only if IPERM=1 or ISEDAV=1 in the same was as $z_b(x)$.

- XBINP(1) and ZBINP(1) = values (m) of x and z of the bottom point at the seaward boundary in the coordinate system (x, z) shown in Fig. 2 where XBINP(1) = 0.0 at the seaward boundary and the water depth below the datum $z = 0$ is given by $-$ ZBINP(1). If IPERM=1 or ISEDAV=1, XPINP(1) = 0.0 and ZPINP(1) = ZBINP(1) are specified in the program because the thickness of a permeable layer or sediment layer is assumed to be zero at the seaward boundary where $z_b(x)$ at $x = 0$ is fixed for the profile evolution computation for IPROFL=1.

- XBINP(J), ZBINP(J) and FBINP(J-1) for J=2,3,…,NBINP where

  XBINP(J) = horizontal (landward) distance (m) of the input bottom point J from the seaward

  boundary $x = 0$ with the distance XBINP(J) increasing with the increase of the integer J.

  ZBINP(J) = bottom elevation $z_b(m)$ of the point J. If the point J is below the datum $z = 0$,

  ZBINP(J) is negative and $-$ ZBINP(J) is the water depth below the datum. If the point J is

  above the datum, ZBINP(J) is positive and corresponds to the bottom elevation of the point J

  above the datum.

  FBINP(J-1) = bottom friction factor f_b of the linear segment between the bottom points (J$-$1)

  and J. The bottom friction factor can be varied to account for the cross-shore variation of

  bottom roughness as shown in Fig. 2.

- XPINP(J), ZPINP(J) for J=2,3,…,NPINP only for IPERM=1 or ISEDAV=1 where

  XPINP(J) = value (m) of the x-coordinate of $z_p(x)$ at the point J.

  ZPINP(J) = value (m) of the z -coordinate of $z_p(x)$ of the point J. The vertical thickness of

  the permeable or sediment layer is given by $h_p = (z_b - z_p)$. If $z_p(x)$ includes a vertical step or

  wall, it should be replaced by a steep slope.

- NWIND = number of data points in the time series of wind speed and direction data only if

  IWIND=1 where the wind data is read in the same way as the wave and water level data for

  ILAB=0.

- TWIND(I), WIND10(I), WINDAN(I) for I=1,2,…, (NWIND+1) only for IWIND=1 where

  TWIND(I) = time (s) for the I-th wind data where TWIND(1) = 0.0 and TWIND (NWIND+1)

  must be the same as the end time of the wave and water level data.

  WIND10(I) = wind speed W_{10} (m/s) at the elevation of 10 m above the sea surface at time =

  TWIND(I).

  WINDAN(I) = wind direction θ_w in degrees (see Fig. 1) at time = TWIND(I).

After the wind data is read, Subroutine 20 TSINTP is called to create the stepped time series

corresponding to ILAB=1.

The following input is required only for the option of IWTRAN=1 which assumes that a bay or

lagoon exists landward of an emerged dune or coastal structure.

- ISWLSL=0 or 1 for the same or different still water levels on the seaward and landward sides.

  If ISWLSL=0, no additional input is required because the landward still water level is taken as

  the seaward still water level specified at the seaward boundary $x = 0$.

- NSLAN = number of data points in the time series of the landward still water level only if

  ISWLSL=1.

- TSLAND(I), SLANIN(I) for I=1,2,…, (NSLAN+1) only if ISWLSL=1 where

  TSLAND(I) = time (s) for the I-th water level data where

  TSLAND(1) = 0.0 and TSLAND(NSLAN+1) must be the same as the end time of the wave

  and seaward water level data.

  SLANIN(I) = landward still water level (m) above the datum $z = 0$ at time = TSLAND(I).

After the water level data is read, Subroutine 20 TSINTP is called to create the stepped time series corresponding to ILAB=1.

10.4 Output

A user of CSHORE must examine the contents of the output file **ODOC** (unit=20 for the WRITE statement) to ensure that the input file has been prepared and read correctly. The contents of this file created in Subroutine 8 **OUTPUT** and at the end of Subroutine 10 **QORATE** if IOVER=1 are self-explanatory. The notations that have not been explained previously are explained in the following.

First, **ODOC** stores the input parameters and variables.

RBZERO = lower limit of the wave-front slope β_r in Eq. (10) where RBZERO = 0.1 specified in Subroutine 2 **INPUT** where this typical value has been used to reduce the number of calibration parameters.

JCREST = crest node of the maximum bottom elevation for the input bottom profile $z_b(x)$. If the crest is horizontal, JCREST corresponds to the landward end of the horizontal crest located at $x = x_c$ in Fig. 5. If IPROFL=1, the nodal location of JCREST may change with the evolution of the bottom profile.

RCREST = input bottom elevation (m) at the node JCREST corresponding to the maximum value of the input $z_b(x)$.

AWD = parameter α in Eq. (92) which expresses the horizontal velocity U as a function of the water depth h in the wet and dry zone where $\alpha = 2$ is specified in Subroutine 4 **PARAM** but this specified value could be calibrated if necessary.

EWD = exceedance probability e used in Eq. (141) for the comparison with measured values

corresponding to 2% of incident irregular waves where e = EWD = 0.01 or 0.015 depending

on IPERM=1 or 0 in Subroutine 4 **PARAM**.

It is noted that JCREST, RCREST, AWD, and EWD are stored only if IOVER=1.

Second, **ODOC** stores the computed quantities at time = TIMEBC(1)=0.0, TIMEBC(2)=,…,

TIMEBC(NTIME+1) for ILAB=1. For ILAB=0, the computed quantities are stored every ten

storage time levels and at the first and last time levels. The stored quantities of the ODOC file

include

JR = most landward node reached by the landward marching computation using the wet model in

Section 4 if IPERM=0 and in Section 6 if IPERM=1.

XR = x-coordinate (m) of the node JR where XR = x_r shown in Fig. 5 for an emerged structure

or beach.

ZR = z-coordinate (m) of the node JR corresponding to the bottom elevation above the datum.

H(JR) = mean water depth $\bar{h}$ (m) at the node JR which must be very small for an emerged

structure or beach if the landward marching computation does not encounter numerical

difficulties.

CSHORE estimates the wave reflection coefficient, assuming that the cross-shore wave energy

flux F_x defined in Eq. (37) is reflected from the node JSWL at the still water shoreline located at

$x = x_{SWL}$ in Fig. 5 and propagates seaward if JR > JSWL (the landward marching computation

has reached above the still water shoreline) and JSWL < JMAX with JMAX = most landward

96

node of the computation domain based on the input bottom geometry. If JSWL = JMAX, the computation domain is submerged and some of the cross-shore wave energy flux is transmitted landward. The wave reflection coefficient REFCOF is estimated as the ratio between σ_{ref} and σ_η at $x=0$ where σ_{ref} is the free surface standard deviation due to the wave energy flux propagating seaward at $x=0$. The wave reflection coefficient is estimated only for IOVER=0 because wave overtopping accompanies onshore wave energy flux.   The estimated wave reflection coefficient may not be very accurate (Kobayashi et al. 2005, 2007a) but is useful in assessing the applicability of CSHORE which neglects reflected waves in its governing equations.

If IOVER=1, Subroutine OUTPUT calls Subroutine 10 QORATE with ICALL=1 to store the following quantities in the file **ODOC**:

JWD = most seaward node of the landward marching computation in the wet and dry zone as explained in relation to Eq. (100).

H1 = mean water depth $\bar{h}_1(m)$ at the node JWD.

JDRY = most landward node in the wet and dry zone which is less than and equal to the maximum node number JMAX in the computation domain.

POTF = wave overtopping probability P_o estimated using the wet probability P_c at the node JCREST as explained below Eq. (102).

QOTF = wave overtopping rate $q_o(m^2/s)$ above the bottom computed using Eq. (102) for an impermeable bottom. For a permeable bottom, QOTF=$(q_o - q_p)$ in Eq. (139).

QP = seepage rate $q_p (m^2/s)$ calculated using Eq. (121) at the node JCREST in Eq. (139). The total overtopping rate is given by $q_o = $ (QOTF + QP).

ITEQO = number of iterations performed to compute the wave overtopping rate q_o.

In addition, the following quantities computed using the empirical equations for wave runup in Section 7 are stored in the file **ODOC** at the specified time levels:

ERMEAN = mean shoreline elevation (m) above the datum $z = 0$ measured by the runup wire where ERMEAN $= \left(\overline{\eta}_r + S \right)$ and $\overline{\eta}_r$ given in Eq. (73) is the mean shoreline elevation above SWL.

SIGRUN = standard deviation σ_r (m) of the shoreline oscillation measured by the runup wire where σ_r is estimated using Eq. (73).

R13 = significant runup height (m) above the datum $z = 0$ corresponding to $\left(R_{1/3} + S \right)$ where $R_{1/3}$ above SWL is estimated using Eq. (75) or (84).

R2P = runup height (m) above the datum $z = 0$ for the 2% exceedance probability where R2P = $\left(R_{2\%} + S \right)$ and $R_{2\%}$ is given by Eq. (79).

If IWTRAN=1 and the landward marching computation reaches the standing water in a bay or lagoon, the quantities related to wave transmission are stored in the file **ODOC** in Subrouting 10 QORATE. The nodes JSL and JMAX are the most seaward and landward nodes, respectively, in the zone of the standing water. The cross-shore locations of these nodes and the mean $\overline{\eta}$ and standard deviation σ_η at these nodes are stored together with the wave

transmission coefficient defined as the ratio between σ_η at the node JMAX and σ_η at the seaward boundary $x = 0$.

If IPROFL=1 and IANGLE=1 (obliquely incident waves), Subroutine OUTPUT integrates the sum of the longshore suspended sediment transport rate q_{sy} (m^2/s) and the longshore bedload transport rate q_{by} (m^2/s) from $x = 0$ to $x = x_r$ in the wet zone where q_{sy} and q_{by} are predicted using Eqs. (52) and (57), respectively. The integrated total longshore sediment transport rate (m^3/s) and the corresponding value of K in the CERC formula (Coastal Engineering Manual 2003) are stored in the file **ODOC**. The breaker location is taken at the cross-shore location of the maximum root-mean-square wave height and the value of K in the CERC formula is supposed to be of the order of 0.8.

If IPROFL=1 and IPERM=1, the profile evolution of a permeable beach or structure is computed. The computed bottom profile $z_b(x)$ at the given time t is compared with the initial bottom profile $z_i(x) = z_b(x)$ at $t = 0$. The eroded area A_e is defined as the area of $\left[z_i(x) - z_b(x) \right] > 0$. The maximum vertical erosion depth d_e is defined at the maximum value of $\left[z_i(x) - z_b(x) \right] > 0$. The damage S_e is defined as $S_e = A_e / D_{n50}^2$ and the normalized erosion depth E is defined as $E = d_e / D_{n50}$ where D_{n50} is the nominal store or sediment diameter. The stability number N_{mo} is defined as $N_{mo} = H_{mo} / \left[(s-1) D_{n50} \right]$ where $H_{mo} = \sqrt{2} H_{rms}$ = spectral significant wave height at $x = 0$ and s = specific gravity of the stone or sediment. The values of

S_e, E and N_{mo} are stored at the specified time levels in the **ODOC** file in Subroutine 8 OUTPUT.

The rest of the output files store the cross-shore variations of computed variables at the specified time levels TIMEBC(I) with I = 1, 2, …, (NTIME+1) for ILAB=1. For ILAB=0, the cross-shore variations are stored every ten storage time levels and at the first and last time levels. Each output file stores the number of nodes and the output time level immediately before the computed variables are stored at the given number of nodes. This will facilitate displaying the computed variables using the output files. It is noted that the CSHORE computer program does not contain any plotting routine.

The file **OBPROF** (unit=21) contains the bottom profile variables at all the nodes with J=1,2,…,JMAX.

XB(J) = cross-shore coordinate x (m) of node J where XB(J) = $(J-1)*\Delta x$ does not change with time.

ZB(J) = vertical coordinate z_b (m) of the bottom elevation at the output time level where the bottom elevation evolves with time if IPROFL=1.

ZP(J) = vertical coordinate z_p (m) of the lower boundary of the permeable layer only if IPERM=1 or ISEDAV=1 where z_p has been assumed to be fixed.

The file **OSETUP** (unit=22) stores the quantities related to the mean and standard deviation of the free surface elevation η for nodes J=1,2,…,JR

XB(J) = cross-shore coordinate x (m) of node J for the plotting convenience.

100

(H(J)+ZB(J)) = sum of the wave setup $\bar{\eta}$ (m) above SWL and storm tide S (m) above the datum at node J [see Eq. (1)].

H(J) = mean water depth $\bar{h}$ (m) at node J.

SIGMA(J) = free surface standard deviation σ_η (m) related to the root-mean-square wave height

$$H_{rms} = \sqrt{8}\sigma_\eta .$$

If IOVER=1, these variables are also stored at nodes J=(JR+1),…,JDRY in the wet and dry zone.

If IWTRAN=1 and the computation reaches the standing water in a bay or lagoon, these variables are stored at nodes J=(JR+1), …, JMAX.

The file **OPARAM** (unit =23) stores XB(J) with nodes J=1,2,…,JR and the following parameters:

WT(J) = intrinsic wave period $T = 2\pi / \omega$ (s) where the angular frequency ω is computed using Eq. (2).

QBREAK(J) = fraction Q of breaking waves computed using Eq. (38).

SIGSTA(J) = ratio $\sigma_* = \sigma_\eta / \bar{h}$ in Eq. (31) whose upper limit is unity in the wet zone.

The file **OXMOME** (unit=24) stores XB(J) with J=1,2,…JR and the following terms in the x-momentum equation (22):

SXXSTA(J) = $\left[S_{xx} / (\rho g) + Q_x^2 / (g\bar{h}) \right]$ (m²) where S_{xx} and Q_x are given in Eqs. (24) and (19), respectively.

TBXSTA(J) = $\tau_{bx} / (\rho g)$ (m) where τ_{bx} is given in Eq. (33).

If IANGLE=1 (obliquely incident waves), the file **OYMOME** (unit=25) stores XB(J) with J=1,2,…,JR and the following terms in the y-momentum equation (23):

SXYSTA(J) = $\left[S_{xy} / (\rho g) + Q_x Q_y / (g\bar{h}) \right]$ (m^2) where S_{xy}, Q_x and Q_y are defined in Eqs. (24),

(19) and (20).

TBYSTA(J) = $\tau_{by} / (\rho g)$ (m) where τ_{by} is given in Eq. (33).

The file **OENERG** (unit=26) stores XB(J) with J=1,2,…,JR and the following terms in the wave action equation (36) or (63) with ω being replaced by T^{-1}:

EFSTA(J)/WT(J) = $\left[E \left(C_g \cos\theta + Q_x / \bar{h} \right) \right] / (\rho g)$ (m^3/s) where E and C_g are given in Eqs. (25)

and (3).

DBSTA(J) = $D_B / (\rho g)$ (m^2/s) where D_B is given by Eq. (38).

DFSTA(J) = $D_f / (\rho g)$ (m^2/s) where D_f is given by Eq. (40).

The file **OXVELO** (unit=27) stores XB(J) with J=1, 2, …, JR and the following cross-shore velocity statistics:

UMEAN(J) = mean velocity $\overline{U}$ (m/s) of the depth-averaged cross-shore velocity U.

USTD(J) = standard deviation σ_U (m/s) of U.

UPMEAN(J) = mean discharge velocity $\overline{U}_p$ (m/s) in the permeable layer computed using Eqs. (70) and (118) if IPERM=1.

If IOVER=1, these variables are also stored at nodes J = (JR+1), …, JDRY in the wet and dry zone. If IWTRAN=1 and the computation reaches the standing water in a bay or lagoon, these variables are stored at nodes J=(JR+1), …, JMAX.

If IANGLE=1, the file **OYVELO** (unit=28) stores XB(J) with J=1, 2, …, JR and the following longshore velocity statistics:

STHETA(J) = $\sin\theta$ with θ = wave angle as defined in Fig. 1 where $\sin\theta$ is computed using Eq. (21).

VMEAN(J) = mean velocity $\overline{V}$ (m/s) of the depth-averaged longshore velocity V.

VSTD(J) = standard deviation σ_V of V.

It is noted that the present wet and dry model is limited to normally incident waves (IANGLE=0).

If IROLL=1, the file **OROLLE** (unit=29) stores XB(J) with J=1, 2, …, JR and

RQ(J) = roller volume flux q_r (m²/s) computed using Eq. (41).

If IROLL=0, $q_r = 0$ and $D_r = D_B$ in Eq. (41).

If IPROFL=1, the file **OBSUSL** (unit=30) stores XB(J) with J=1,2, …, JR and the following variables related to sediment transport:

PB(J) = probability P_b of sediment movement.

PS(J) = probability P_s of sediment suspension.

VS(J) = suspended sediment volume V_s (m) per unit horizontal bottom area.

If IOVER=1, these variables are also stored at nodes J = (JR+1), …, JDRY in the wet and dry zone. If IWTRAN=1 and the computation reaches the standing water in a bay or lagoon, these variables are stored at nodes J=(JR+1), …, JMAX.

If IPERM=1,the file **OPORUS** (unit=31) stores XB(J) with J=1, 2, …, JR and the following variables related to the permeable layers in the wet zone:

UPSTD(J) = standard velocity σ_p (m/s) of the discharge velocity computed using Eq. (72).

DPSTA(J) = $D_p / (\rho g)$ (m²/s) where the energy dissipation rate D_p due to flow resistance in the permeable layer is computed using Eq. (68).

If IPROFL=1, the file **OCROSS** (unit=32) stores XB(J) with J=1, 2, …, JMAX and the following cross-shore sediment transport rates:

QBX(J) = cross-shore bedload transport rate q_{bx} (m²/s).

QSX(J) = cross-shore suspended sediment transport rate q_{sx} (m²/s).

(QBX(J) + QSX(J)) = cross-shore total sediment transport rate q_x (m²/s).

It is noted that the transport rates are stored at all the nodes but the rates are zero in the completely dry zone.

If IPROFL=1 and IANGLE=1, the file **OLONGS** (unit=33) stores XB(J) with J=1,2, … JMAX and the following longshore sediment transport rates:

QBY(J) = longshore bedload transport rate q_{by} (m²/s).

QSY(J) = longshore suspended sediment transport rate q_{sy} (m²/s).

(QBY(J) + QSY(J)) = longshore total sediment transport rate q_y (m²/s).

If IOVER=1, the file **OSWASH** (unit=34) stores XB(J) with J= 1,2, …, JDRY or JMAX and the following quantities related to the wet and dry zone:

PWET(J) = wet probability P_w at node J corresponding to the ratio between the wet duration and
the total duration at this node.

QP(J) = water flux inside the permeable layer in Eqs. (62) and (121) if IPERM=1.

If IOVER=1, the file **OSWASE** (unit=35) stores XB(J) with J = JWD, …, JDRY and the following quantities in Eqs. (141) and (142):

HEWD(J) = water depth h_e (m) corresponding to the exceedance probability e = EWD.

UEWD(J) = cross-shore velocity U_e (m/s) corresponding to the exceedance probability e

QEWD(J) = cross-shore volume flux q_e (m²/s) corresponding to the exceedance probability e.

If IPROFL=1 and IOVER=1, the file **OTIMSE** (unit = 36) stores the following time series in **Main Program:**

TSTOUT = time t (s) starting from $t = 0$ for the storage of time series.

TSQO(I) = wave overtopping rate q_o (m²/s).

TSQBX(I) = cross-shore bedload transport rate q_{bx} (m^2/s) at the landward end of the computation domain.

TSQSX(I) = cross-shore suspended sediment transport rates q_{sx} (m^2/s) at the landward end of the computation domain.

The file **OMESSG** (unit=40) stores warning and error messages generated during the computation. This file has been used to find input errors and improve the numerical iteration methods adopted in CSHORE.

A user of CSHORE may not be interested in the computed results in all the output files but should examine all the appropriate output files and ensure that the computed results are realistic physically. This is especially true if CSHORE is applied to new problems where the previous applications of CSHORE have been summarized in Section 2.

11. CONCLUSIONS

The horizontally two-dimensional model C2SHORE and the cross-shore model CSHORE are presented. The numerical model C2SHORE is based on the spectral wave model STWAVE (Smith et al. 2001) for the prediction of the directional wave transformation, radiation stresses, and wave-induced volume fluxes and the circulation model, which is a simplified version of SHORECIRC (Svendsen et al. 2002) for irregular waves, for the prediction of the wave setup and depth-averaged current velocities. The combined wave current model CSHORE based on

the time-averaged continuity, cross-shore momentum, longshore momentum, wave action and roller energy equations predicts the cross-shore variations of the mean and standard deviation of the free surface elevation and depth-averaged cross-shore and longshore velocities under normally or obliquely incident irregular breaking waves. Both models use the same sediment transport formulas for the cross-shore and longshore transport rates of suspended sediment and bedload on sand beaches. These formulas are relatively simple and require the hydrodynamic input variables which can be predicted efficiently and fairly accurately using existing wave and current models. The numerical model C2SHORE has been compared only with one set of field data partly because of its complexity and partly because of lack of bench mark data. The much simpler model CSHORE has been compared with a number of small-scale and large-scale laboratory data and field data. CSHORE has been extended to the intermittently wet and dry zone for the prediction of wave overwash of a dune and deformation of a low-crested stone structure.

The computer program CSHORE has been developed with collaboration of a number of graduate students and visiting researchers for the last 10 years. The essential parts of CSHORE and the details of the input and output are described in this report in order to facilitate the use of CSHORE by the broad coastal community. CSHORE based on the time-averaged governing equations is much easier to apply than the corresponding time-dependent model developed by the author of this report (e.g., Kobayashi and Wurjanto 1990, 1992). A user of CSHORE for a specific problem should read references in Section 2 that are related to the user's specific problem because the user will need to interpret the computed results. CSHORE provides various options but only certain combinations of the options have been examined in the previous

computations in Section 2. Finally, CSHORE is being compared with a gravel beach experiment and a beach recovery experiment and will be extended to allow gradual alongshore variations.

REFERENCES

Apotsos, A., Raubenheimer, B., Elgar, S., and Guza, R.T. (2008). "Testing and calibrating parametric wave transformation models on natural beaches." Coastal Eng., 55, 224-235.

Bagnold, R.A. (1966). "An approach to the sediment transport problem from general physics." U.S. Geol. Surv., Prof. Paper 422-I.

Bailard, J.A. (1981). "An energetics total load sediment transport model for a plane sloping beach." J. Geophys. Res., 86, 10,938-10,954.

Battjes, J.A., and Stive, M.J.F. (1985). "Calibration and verification of a dissipation model for random breaking waves." J. Geophys. Res., 90(C5), 9159-9167.

Becker, J.M., Firing, Y.L., Aucan, J., Holman, R., Merrifield, M., and Pawlak, G. (2007). "Video-based observations of nearshore sand ripples and ripple migration." J. Geophys. Res., 112, C01007, doi10.1029/2005JC003451.

Chaudhry, M.H. (1993). Open-channel Flow. Prentice Hall, Englewood Cliffs, NJ.

Coastal Engineering Manual. (2003). Coastal and Hydraulics Lab, US Army Engineer Research and Development Center, Vicksburg, Miss.

Dalrymple, R.A. (1988). "Model for refraction of water waves." J. Waterway, Port, Coastal, Ocean Eng., 114(4), 423-435.

Dean, R.G. (1991). "Equilibrium beach profile: Characteristics and applications." J. Coastal Res., 7, 53-84.

Dohmen-Janssen, C.M., and Hanes, D.H. (2002). "Sheet flow dynamics under monochromatic nonbreaking waves." J. Geophys. Res., 107(C10), 3149, doi:10.1029/2001JC001045.

Dohmen-Janssen, C.M., Kroekenstoel, D.F., Hassan, W.N., and Ribberink, J.S. (2002). "Phase lags in oscillatory sheet flow: Experiments and bedload modeling." Coastal Eng., 47, 295-327.

EurOtop Manual (2007). "Wave overtopping of sea defences and related structures: Assessment manual." www.overtopping-manual.com.

Farhadzadeh, A., Kobayashi, N., and Melby, J.A. (2009). "Wave overtopping and damage progression on rubble mound structures." Research Rep. No. CACR-09-05, Center for Applied Coastal research, Univ. of Delaware, Newark, Del.

Farhadzadeh, A., Kobayashi, N., Melby, J.A., and Ricottilli, C. (2007). "Experiments and numerical modeling of wave overtopping and overflow on dikes." Research Rep. No. CACR-07-02, Center for Applied Coastal Research, Univ. of Delaware, Newark, Del.

Feddersen, F., Guza, R.T., Elgar, S., and Herbers, T.H.C. (2000). "Velocity moments in alongshore bottom stress parameterization." J. Geophys. Res., 105(C4), 8673-8686.

Figlus, J., Kobayashi, N., Gralher, C., and Iranzo, V. (2009). "Experimental and numerical study on transition from minor to major wave overwash." Research Rep. No. CACR-09-04, Center for Applied Coastal Research, Univ. of Delaware, Newark, Del.

Gallagher, E.L., Elgar, S., and Guza, R.T. (1998). "Observations of sand bar evolution on a natural beach." J. Geophys. Res., 103, 3203-3215.

Henderson, S.M., Allen, J.S., and Newberger, P.A. (2004). "Nearshore bar migration predicted by an eddy-diffusive boundary layer model." J. Geophys. Res., 109, C06024, doi:10.1029/2003JC02137.

Hoefel, F., and Elgar, S. (2003). "Wave-induced sediment transport and sandbar migration." Science, 299, 1885-1887.

Holland, K.T., Holman, R.A., and Sallenger, A.H., Jr. (1991). "Estimation of overwash bore velocities using video techniques." Proc. Coastal Sediments'91, ASCE, Reston, Va., 489-497.

Jiménez, J.A., and Madsen, O.S. (2003). "A simple formula to estimate settling velocity of natural sediments." J. Waterway, Port, Coastal, Ocean Eng., 129(2), 70-78.

Kamphuis, J.S. (1991). "Alongshore sediment transport rate." J. Waterway, Port, Coastal, Ocean Eng., 117(6), 624-640.

Kobayashi, N. (1999). "Wave runup and overtopping on beaches and coastal structures." Advances in Coastal and Ocean Engineering, World Scientific, Singapore, 5, 95-154.

Kobayashi, N., and de los Santos, F.J. (2007). "Irregular wave seepage and overtopping of permeable slopes." J. Waterway, Port, Coastal, Ocean Eng., 133(4), 245-254.

Kobayashi, N., and Farhadzadeh, A. (2008). "Cross-shore numerical model CSHORE for waves, currents, sediment transport and beach profile evolution." Research Rep. No. CACR-08-01, Center for Applied Coastal Research, Univ. of Delaware, Newark, Del.

Kobayashi, N., and Johnson, B.D. (2001). "Sand suspension, storage, advection, and settling in surf and swash zones." J. Geophys. Res., 106, 9363-9376.

Kobayashi, N., and Otta, A.K. (1987). "Hydraulic stability analysis of armor units." J. Waterway, Port, Coastal, Ocean Eng., 113(2), 171-186.

Kobayashi, N., and Tega, Y. (2002). "Sand suspension and transport on equilibrium beach." J. Waterway, Port, Coastal, Ocean Eng., 128(6), 234-248.

Kobayashi, N., and Wurjanto, A. (1990). "Numerical model for waves on rough permeable slopes." J. Coastal Res., SI(7), 149-166.

Kobayashi, N., and Wurjanto, A. (1992). "Irregular wave setup and run-up on beaches." J. Waterway, Port, Coastal, Ocean Eng., 118(4), 368-386.

Kobayashi, N., DeSilva, G.S., and Watson, K.D. (1989). "Wave transformation and swash oscillation on gentle and steep slopes." J. Geophys. Res., 94(C1), 951-966.

Kobayashi, N., Zhao, H., and Tega, Y. (2005). "Suspended sand transport in surf zones." J. Geophys. Res., 110, C12009, doi:10.1029/2004JC002853.

Kobayashi, N., Agarwal, A., and Johnson, B.D. (2007a). "Longshore current and sediment transport on beaches." J. Waterway, Port, Coastal, Ocean Eng., 133(4), 296-304.

Kobayashi, N., Farhadzadeh, A., and Melby, J.A. (2007c). "Structures of storm surge disaster prevention." Proc. 4th International Workshop on Coastal Disaster Prevention, Yokohama, Japan, 41-49.

Kobayashi, N., Payo, A., and Schmied, L. (2008a). "Cross-shore suspended sand and bedload transport on beaches." J. Geophys. Res., 113, C07001, doi:10.1029/2007JC004203.

Kobayashi, N., de los Santos, F.J., and Kearney, P.G. (2008b). "Time-averaged probabilistic model for irregular wave runup on permeable slopes." J. Wateway, Port, Coastal, Ocean Eng., 134(2), 88-96.

Kobayashi, N., Payo, A., and Johnson, B.D. (2009a). "Suspended sand and bedload transport on beaches." Handbook of Coastal and Ocean Engineering, World Scientific, Singapore, Chapter 28, 807-823.

Kobayashi, N., Pozueta, B., and Melby, J.A. (2003). "Performance of coastal structures against sequences of hurricanes." J. Waterway, Port, Coastal, Ocean Eng., 129(5), 219-228.

Kobayashi, N., Herrman, M.N., Johnson, B.D., and Orzech, M.D. (1998). "Probability distribution of surface elevation in surf and swash zones." J. Waterway, Port, Coastal, Ocean Eng., 124(3), 99-107.

Kobayashi, N., Meigs, L.E., Ota, T., and Melby, J.A. (2007b). "Irregular breaking wave transmission over submerged porous breakwaters." J. Waterway, Port, Coastal, Ocean Eng., 133(2), 104-116.

Kobayashi, N., Buck, M., Payo, A., and Johnson, B.D. (2009b). "Berm and dune erosion during a storm." J. Waterway, Port, Coastal, Ocean Eng., 135(1), 1-10.

Kobayashi, N., Farhadzadeh, A., Melby, J., Johnson, B., and Gravens, M. (2010). "Wave overtopping of levees and overwash of dunes." J. Coastal Res., (in press).

Kriebel, D.L., and Dean, R.G. (1985). "Numerical simulation of time-dependent beach and dune erosion." Coastal. Eng., 9, 221-245.

Large, W.G., and Pond, S. (1981). "Open ocean momentum flux measurements in moderate to strong winds." J. Phys. Oceanography, 11, 324-336.

Lentz, S., Guza, R.T., Elgar, S., Feddersen, F., and Herbers, T.H.C. (1999). "Momentum balances on the North Carolina inner shelf." J. Geophys. Res., 104(C8), 18,205-18,226.

Losada, I.J., Lara, J.L., Guanche, R., and Gonzalez-Ondina, J.M. (2008). "Numerical analysis of wave overtopping of rubble mound breakwaters." Coastal Eng., 55, 47-62.

Madsen, O.S., and Grant, W.D. (1976). "Quantitative description of sediment transport by waves." Coastal Engineering 1976, Proc. 15th Coastal Engineering Conf., ASCE, Reston, Va., 1093-1112.

Madsen, O.S., Chisholm, T.A., and Wright, L.D. (1994). "Suspended sediment transport in inner shelf waters during extreme storms." Coastal Engineering 1994, Proc. 24th Coastal Engineering Conf., ASCE, Reston, Va., 1849-1864.

Masselink, G., Austin, M.J., O'Hare, T.J., and Russell, P.E. (2007). "Geometry and dynamics of wave ripples in the nearshore zone of a coarse sandy beach." J. Geophys. Res., 112, C10022, doi:10.1029/2006JC003839.

Mei, C.C. (1989). The applied dynamics of ocean surface waves. World Scientific, Singapore.

Melby, J.A., and Kobayashi, N. (1998). "Progression and variability of damage on rubble mound breakwaters." J. Waterway, Port, Coastal, Ocean Eng., 124(6), 286-294.

Nairn, R.B., and Southgate, H.N. (1993). "Deterministic profile modelling of nearshore processes. Part 2. Sediment transport and beach profile development." Coastal Eng., 19, 57-96.

Neves, M.G., Reis, M.T., Losada, I.J., and Hu, K. (2008). "Wave overtopping of Póvoa de Varzin breakwater: Physical and numerical simulations." J. Waterway, Port, Coastal, Ocean Eng., 134(4), 226-236.

Norton, P.A., and Holmes, P. (1992). "Armor displacements on reshaping breakwaters." Coastal Engineering 1992, Proc. 23rd Coastal Engineering Conf., ASCE, Reston, Va., 1448-1460.

Payo, A,. Kobayashi, N., and Yamada, F. (2009). "Suspended sand transport along pier depression." J. Waterway, Port, Coastal, Ocean Eng., 135(5), 245-249.

Phillips, O.M. (1977). The dynamics of the upper ocean. Cambridge Univ. Press, Cambridge, U.K.

Powell, M.D., Vickery, P.J., and Reinhold, T.A. (2003). "Reduced drag coefficient for high wind speeds in tropical cyclones." Nature, 422, 279-283.

Press, W.H., Flannery, B.P., Teukolsky, S.A., and Vettering, W.T. (1989). Numerical recipes. The art of scientific computing. Cambridge Univ. Press, New York, NY.

Ribberink, J.S. (1998). "Bed-load transport for steady flow and unsteady oscillatory flows." Coastal Eng., 34, 59-82.

Ribberink, J.S., and Al-Salem, A.A. (1994). "Sediment transport in oscillatory boundary layers in cases of rippled beds and sheet flow." J. Geophys. Res., 99, 12,707-12,727.

Ruessink, B.G., Miles, J.R., Feddersen, F., Guza, R.T., and Elgar, S. (2001). "Modeling the alongshore current on barred beaches." J. Geophys. Res., 106(C10), 22,451-22,463.

Seymour, R., Guza, R.T., O'Reilly, W., and Elgar, S. (2005). "Rapid erosion of a small southern California beach fill." Coastal Eng., 52, 151-158.

Shi, F., Kirby, J.T., and Hanes, D.M. (2007). "An efficient model-splitting method for a curvilinear nearshore circulation model." Coastal Eng., 54, 811-824.

Shi, F., Johnson, B., and Kobayashi, N. (2008). "2DH modeling of waves, currents and sediment transport at FRF during Hurricane Isabel." 2008 Ocean Sciences Meeting, American Geophysical Union, Orlando, Florida.

Smith, J.M., Sherlock, A.R., and Resio, D.T. (2001). "STWAVE: Steady-state spectral wave model user's manual for STWAVE, version 3.0." ERDC/CHL SR-01-1, Coastal and Hydraulics Laboratory, US Army Corps of Engineers, Vicksburg, Miss.

Schüttrumpf, H., and Oumeraci, H. (2005). "Layer thickness and velocities of wave overtopping flow at sea dikes." Coastal Eng., 52, 473-495.

Svendsen, I.A., Haas, K., and Zhao, Q. (2002). "Quasi-3D nearshore circulation model SHORECIRC version 2.0." Res. Rep. No. CACR-02-01, Center for Applied Coastal Research, Univ. of Delaware, Newark, Del.

Tega, Y. and Kobayashi, N. (1996). "Wave overwash of subaerial dunes." Coastal Engineering 1996, Proc. 25th Coastal Engineering Conf., ASCE, Reston, Va., 4148-4160.

Tega, Y., and Kobayashi, N. (1999). "Numerical modeling of overwashed dune profiles." Proc. Coastal Sediments'99, ASCE, Reston, Va. 1355-1370.

Thornton, E.G., Humiston, R.T., and Birkemeier, W. (1996). "Bar/trough generation on a natural beach." J. Geophys. Res., 101, 12,097-12,110.

Trowbridge, J., and Young, D. (1989). "Sand transport by unbroken water waves under sheet flow conditions." J. Geophys. Res., 94, 10,971-10,991.

van Gent, M.R.A. (1995). "Porous flow through rubble-mound material." J. Waterway, Port, Coastal, Ocean Eng., 121(3), 176-181.

van Gent, M.R.A. (2001). "Wave runup on dikes with shallow foreshores." J. Waterway, Port, Coastal, Ocean Eng., 127(5), 254-262.

van Gent, M.R.A. (2002a). "Wave overtopping events at dikes." Coastal Engineering 2002, Proc. 28th Coastal Engineering Conf., World Scientific, Singapore, 2203-2215.

van Gent, M.R.A. (2002b). "Low-exceedance wave overtopping events: Measurements of velocities and the thickness of water-layers on the crest and inner slope of dikes." Delft Cluster Report DC030202/H3803, Delft Hydraulics, Delft, The Netherlands.

van Gent, M.R.A., Coeveld, E.M., Walstra, D.J.R., van de Graaff, J., Steetzel, H.J., and Boers, M. (2006). "Dune erosion tests to study the influence of wave periods." Coastal

Engineering 2006, Proc. 30th Coastal Engineering Conf., World Scientific, Singapore, 2779-2791.

van Rijn, L.C., Walstra, D.J.R., Grasmeijer, B., Sutherland, J., Pan, S., and Sierra, J.P. (2003). "The predictability of cross-shore bed evolution of sandy beaches at the time scale of storms and seasons using process-based Profile models." Coastal Eng., 47, 295-327.

Wurjanto, A., and Kobayashi, N. (1993). "Irregular wave reflection and runup on permeable slopes." J. Waterway, Port, Coastal, Ocean Eng., 119(5), 537-557.